UNIVERSITÀ
DEGLI STUDI
DI BRESCIA

DOTTORATO DI RICERCA IN INTELLIGENZA ARTIFICIALE IN MEDICINA E INNOVAZIONE NELLA RICERCA CLINICA E METODOLOGICA

settore scientifico disciplinare MED/31

XXXVI CICLO

BONE REGENERATION OF THE CRANIOFACIAL SKELETON WITH BIOENGINEERED SCAFFOLDS

DOTTORANDO

Dott. Stefano Taboni

SUPERVISORE

Prof.ssa Luciana Sartore

Summary

ABSTRACT *(English version)*

Reconstruction of maxillofacial skeleton defects is a surgical challenge, and microvascular reconstruction is the current gold standard. The field of tissue bioengineering has been providing an increasing number of alternative strategies for bone reconstruction. We performed a series of preclinical studies to assess the performance of bioengineered scaffolds in craniofacial bone regeneration. In our pilot study an hydrogel made of polyethylene glycol-chitosan (HyCh) and a core-shell combination of poly(L-lactic acid)/poly(ε-caprolactone) and HyCh (PLA-PCL-HyCh), seeded with different concentrations of human mesenchymal stromal cells (hMSCs) (*i.e.* 1000, 2000, and 3000 cells/mm^3), has been explored in non-critical size mandibular defects in a rabbit model. The bone regenerative properties of the bioengineered scaffolds were analyzed by *in vivo* radiological examinations and *ex vivo* radiological, histomorphological, and immunohistochemical analyses. We demonstrate that bone regeneration can be boosted by scaffold- and seeded scaffold-reconstruction, achieving, respectively, 50% and 70% restoration of presurgical bone density in 120 days, compared to 40% restoration seen in spontaneous regeneration. These results helped to establish a baseline reference for further experiments and we started to search for an optimization of the regenerative performance. We tried to optimize the baseline model though the application of an allograft model (*i.e.* seeding rabbit mesenchymal stromal cells [rMSCs] instead of hMSCs) and though the local administration of BMP-2 (*i.e.* bioengineered scaffolds seeded with hMSCs, implemented with BMP-2). Unfortunately the experimental results could not overcome the outcome of 70% restoration of presurgical bone density in 120 days. Afterwards our team developed and produced a new hybrid core-shell composite scaffolds in 3D-printed PLA-HyCH with excellent mechanical properties. We introduced a the new composite scaffold in our experiments, testing the possibility of regenerating of critical size defects, but once again we could not obtain a better performance than our reference value. This finding probably was consequence of suboptimal fixation of the scaffolds at level of the surgical defects. Moreover, some ancillary studies were performed in order to clarify some issues of the bone regeneration: 1) the feasibility of the reconstruction of a segmental mandibular defect though a

bioresorbable hybrid core-shell composite scaffold was proved with a long follow up (*i.e.* 3 months) of the animal without any major complication; 2) a valid animal model of mandibular osteoradionecrosis with an excellent correlation between dose and biological damage was developed, but, from the regenerative standpoint, the scaffold-hMSC model could not highly catalyze the bone repair of bone defects in this particular setting; 3) a preliminary investigation focused on the interaction between hMSCs and tumor cells was accomplished, and, from the few data obtained at the moment, no evidence supported the hypothesis that hMSCs could promote tumor growth.

ABSTRACT *(Italian version)*

La ricostruzione dei difetti ossei del massiccio facciale rappresenta una sfida chirurgica e attualmente la miglior soluzione, in uso nella pratica clinica, consiste nell'impiego di lembi liberi microchirurgici. Il campo della bioingegneria sta crescendo notevolmente e fornisce alcune alternative alla ricostruzione ossea. Durante il dottorato sono stati condotti una serie di studi preclinici al fine di valutare la performance degli scaffold bioingegnerizzati nella rigenerazione ossea del distretto craniofacciale. Nello studio pilota due tipi di scaffold (un idrogelo costituito da polietilen glicole-chitosano [HyCh] e uno scaffold nato dalla combinazione di acido polilattico, policaprolattone e HyCh [PLA-PCL-HyCh]), seminati con cellule staminali mesenchimali umane (hMSCs) in diverse concentrazioni (*i.e.* 1000, 2000, and 3000 cells/mm 3), sono stati testati per la ricostruzione di difetti mandibolari non critici nel modello animale di coniglio. Le proprietà rigenerative degli scaffold bioingegnerizzati sono state analizzate con studi radiologici in vivo ed analisi radiologiche ed istologiche ex vivo. E' stato dimostrato che la rigenerazione ossea può essere incrementata significativamente attraverso l'utilizzo di una ricostruzione con scaffold o con scaffold seminato, ottenendo rispettivamente una rigenerazione ossea del 50% e del 70% del sito chirurgico in 120 giorni, confrontata con il 40% che si ottiene con la rigenerazione spontanea. Questi risultati hanno permesso di stabilire un riferimento di base per ulteriori esperimenti volti all'ottimizzazione della performance rigenerativa. E' stato avviato un primo tentativo di ottimizzare il modello di base con un trapianto allograft di cellule staminali (*i.e.* rabbit mesenchymal stromal cells [rMSCs] in sostituzione delle hMSCs) e con la somministrazione topica di BMP-2 (*i.e.* scaffolds seminati con hMSCs a cui si aggiunge BMP-2). Purtroppo i risultati sperimentali così ottenuti non hanno superato il riferimento di base. Studi successivi sono stati dedicati alla progettazione e sviluppo di un nuovo tipo di scaffold composito con architettura core-shell. Tale scaffold grazie alla struttura reticolare del core prodotto mediante stampante 3D presenta notevole versatilità ed eccellenti proprietà meccaniche. Il nuovo scaffold è stato introdotto per testare la possibilità di rigenerare difetti con dimensioni critiche. I risultati ottenuti non sono stati completamente soddisfacenti a causa di

problematiche legate al fissaggio subottimale dello scaffold a livello del difetto chirurgico. Infine sono stati eseguiti diversi studi ancillari per fare chiarezza in alcune problematiche della rigenerazione ossea: 1) è stata dimostrata la fattibilità della ricostruzione con scaffold bioriassorbibile di un difetto segmentale di mandibola nel coniglio con un lungo follow up (*i.e.* 3 months) nessuna complicanza maggiore; 2) è stato sviluppato un valido modello di osteoradionecrosi mandibolare con ottima correlazione dose-effetto biologico anche se, dal punto di vista rigenerativo, lo scaffold seminato con hMSCs non è riuscito a promuovere il processo neo-osteogenetico; 3) è stato condotto uno studio preliminare per investigare l'interazione tra le hMSCs e le cellule tumorali e al momento non sono emerse evidenze che supportino la teoria che le hMSCs possano favorire la crescita tumorale.

RATIONAL OF THE PROJECT

Reconstruction of bone-including defects following ablation or trauma of the head and neck is a surgical challenge in view of several issues. In fact, the reconstruction must provide adequate mechanical support, maintenance of basic physiological functions (*i.e.* breathing, swallowing, speaking, binocular view), and acceptable morphological-aesthetic profile. This problem involves several clinical scenarios of the head and neck oncology, as surgical resection for oral, sinonasal, orbit, and skull base cancer frequently includes the removal of a non-negligible portion of the craniofacial skeleton. Currently, the gold standard method to assess this challenge is the reconstruction with re-vascularized bone-containing free flaps. These microvascular reconstructions provide optimal results by virtue of the vitality of the bone tissue that is used. This characteristic renders re-vascularized bone-containing free flaps far more appealing than bony autografts, especially when adjuvant treatments are required. On the other hand, these reconstructions are technically demanding, requiring high expertise, a considerable time for harvesting and anastomosing the pedicle, and a non-negligible dose of handicraft skills that need several years to be developed. Moreover, the donor site morbidity, though potentially minimized in expert hands, can be considered a further unavoidable drawback of this technique.

The field of bioengineering has been providing a constantly increasing number of interesting evidences during the last decades. The possibility of creating bony, cartilaginous, and mucosal tissues is arousing a particular interest in several surgical specialties, including head and neck surgery and neurosurgery.[1] As a matter of fact, the establishment of bioengineering protocols applicable to the clinical setting would have a dramatic impact on all the medical disciplines, ranging from surgical oncology to organ transplantation, trauma surgery, cardiovascular interventions, orthopedics, dentistry, and many others.

The paradigm of bone tissue bioengineering is a “triad” of factors including: 1) an adequate scaffold serving as temporary framework for new tissue formation; 2) stem cells able to proliferate and differentiate in progenitors of specialized tissues (i.e. bone, cartilage, epithelium); 3) and efficient

biochemical or physical triggers able to induce and maintain the process of new tissue formation.[2] A large number of systematic reviews offer a landscape of available materials,[3-6] stem cells,[3, 6, 7] and trigger factors,[3] along with several variants in terms of production, refinement, implementation, and combination of these fundamentals.[5, 8] The remarkable quantity of preclinical data obtained *in vitro* and *in vivo* has been recently followed by few but significant pieces of evidence in humans, which reinforce the belief of a possible translation of these interesting techniques into the clinical practice.[3,4,9]

Ideally, a scaffold intended for bone reconstruction conveys a large number of well-defined properties: 1) it must be biocompatible, thus non-eliciting excessive adverse reactions such inflammation, nor causing organ toxicity; 2) it has to be bioresorbable and/or biodegradable by contact with biological fluids (i.e. blood, serum) and surrounding tissues; 3) the timing of resorption/degradation should be synchronous with that of new tissue formation; 4) the scaffold must have sufficient mechanical properties (i.e. stiffness) to temporarily substitute the missing bone and permit essential physiological functions; 5) it has to be osteoinductive and osteoconductive,[10] which means promoting new bone formation (i.e. with specific structural frameworks, implementation of inorganic nanoparticles, or with mechanical stimulation as vibration)[11-14] and favorite its growth into the volume of the scaffold (i.e. by means of porosity),[15] respectively; 6) finally, the scaffold should be prone to be amply vascularized by neoangiogenesis, which is essential for several types of new tissue formation, especially for the bone. A basic concept of tissue bioengineering is the biomimicry, consisting of the imitation of biological architecture and/or chemical composition to augment the similarity of the newly formed tissue compared to the natural one.

Several materials have been thoroughly studied and modified with the intent of finding the most adapt for bone tissue bioengineering. Among all, the possibility of computer-aided designing (CAD) and subsequently computer-aided manufacturing (CAM) a certain material is of utmost interest when considering the possible clinical applications of such biomaterials.[11] In fact, some difficulties encountered during surgery (*i.e.* perfect matching between the edges of reconstruction of

skull base of craniofacial defects) could be promptly overcome applying the CAD-CAM method to create a customized bioengineered scaffold. Moreover, the matching between the surfaces of the scaffold and boundaries of the defect is well recognized as key factor to allow new bone formation.[16] However, a material that is suitable for CAD-CAM and carries all the six above-mentioned properties is not currently available.[17, 18] This poses several limitations in terms of bioengineered reconstruction of complex bone-including defects, where the area of new bone formation is adjacent to a heterogeneous range of tissues. However, several preclinical evidences suggest that biomaterials are differently conforming to sustain new tissue formation based on their specific properties. For instance, collagen and hydrogel are remarkably suitable for neovascularization but require some modifications to favor new bone formation. On the contrary, polycoprolactone, polylactate, and tetracalcium phosphate are osteoinductive *per se* but less prone to be vascularized. Consequently, one can hypothesize to combine biomaterials carrying complementary features to create an ideal scaffold for complex reconstructions, in keeping with the concept of biomimicry.[17] The same line of reasoning can be applied to the other two basic ingredients of bioengineering, namely stem cells and growth stimuli.[17] Some evidences proved the successfulness of this approach.[19-21]

The main limitation of data coming from the current literature on this topic is the absence of enough simulation of the real problems to be faced in the clinical setting. Most of the experiments that have been published were aimed at demonstrating and optimizing the process of new tissue formation. Some attempts on large animal provided encouraging proofs that bioengineered scaffolds work also in large size defects. Complementary, pioneering reports on human patients suggest the feasibility of the technique, though limitedly to relatively simple surgical scenarios. However, few studies simulated complex clinical problems such as the reconstruction of large defects following maxillectomy or mandibulectomy. Preclinical high-quality data on the process of using CAD-CAM bioengineered scaffold for primary reconstruction of bone-containing defects in critical areas are therefore missing. Experiments simulating the entire workflow of this technique constitute a mandatory step that is preparatory to the translation towards the clinical setting.[18, 22] Such experiments

should be designed with a twofold perspective: on one hand, the overall process should be concretely assessed in terms of feasibility, timing, costs, and safety; on the other, limitations emerging throughout the workflow could be attentively highlighted and subsequently faced during future research.

Up to date, there are few commercialized products available for skeletal regeneration, including facial regeneration. Bone Graft (Medtronic and Wyeth) product were approved in USA in lumbar interbody spinal fusion procedures. The approval was based on multicentric, randomized, large-scale data, consisting in 2-year study of 279 degenerative disc disease patients implanted with the device or treated with traditional autograft procedures. The bioengineered Bone Graft recipients showed a trend towards higher fusion rates compared with the autograft patients at 24 months (94.5 *vs* 88.7%). In addition, patients implanted with Bone Graft device spent less time in the operating room and had reduced blood loss during surgery than the autograft patients. Although Bone Graft and autograft patients had similar levels of low back pain relief, the Bone Graft device patients did not experience hip donor site pain.[23] Another commercially available product is Osigraft (Stryker Biotech), which has been tested in a prospective phase II clinical trial on 9 unilateral and 2 bilateral alveolar clefts, obtaining good bone formation and a maxillary growth similar to cases grafted with autogenous bone. No long-term complications or abnormal pattern of bone formation were detected over 10 years of follow up.[24] These products are interesting devices, they have been approved by FDA. Nevertheless, only Osigraft has been investigated for bone regeneration in the maxilla-facial skeleton, and the structures of-these devices are not mechanically adequate for substituting large bone defects.

References

1. Tollemar V, Collier ZJ, Mohammed MK, et al. Stem cells, growth factors and scaffolds in craniofacial regenerative medicine. Genes & diseases 2016; 3:56-71.
2. Ho-Shui-Ling A, Bolander J, Rustom LE, et al. Bone regeneration strategies: Engineered scaffolds, bioactive molecules and stem cells current stage and future perspectives. Biomaterials 2018; 180:143-162.
3. Roffi A, Krishnakumar GS, Gostynska N, et al. The Role of Three-Dimensional Scaffolds in Treating Long Bone Defects: Evidence from Preclinical and Clinical Literature-A Systematic Review. Biomed Res Int 2017; 2017:8074178.
4. Hosseinpour S, Ghazizadeh Ahsaie M, Rezai Rad M, et al. Application of selected scaffolds for bone tissue engineering: a systematic review. Oral Maxillofac Surg 2017; 21:109-129.
5. Kim HD, Amirthalingam S, Kim SL, et al. Biomimetic Materials and Fabrication Approaches for Bone Tissue Engineering. Adv Healthc Mater 2017; 6.
6. Pilipchuk SP, Plonka AB, Monje A, et al. Tissue engineering for bone regeneration and osseointegration in the oral cavity. Dental materials : official publication of the Academy of Dental Materials 2015; 31:317-338.
7. Romagnoli C, and Brandi ML. Adipose mesenchymal stem cells in the field of bone tissue engineering. World J Stem Cells 2014; 6:144-152.
8. Motamedian SR, Hosseinpour S, Ahsaie MG, et al. Smart scaffolds in bone tissue engineering: A systematic review of literature. World J Stem Cells 2015; 7:657-668.
9. Zeng JH, Liu SW, Xiong L, et al. Scaffolds for the repair of bone defects in clinical studies: a systematic review. J Orthop Surg Res 2018; 13:33.
10. Albrektsson T, and Johansson C. Osteoinduction, osteoconduction and osseointegration. Eur Spine J 2001; 10 Suppl 2:S96-101.
11. Yuan H, Xing K, and Hsu HY. Trinity of Three-Dimensional (3D) Scaffold, Vibration, and 3D Printing on Cell Culture Application: A Systematic Review and Indicating Future Direction. Bioengineering (Basel) 2018; 5.
12. Ren X, Bischoff D, Weisgerber DW, et al. Osteogenesis on nanoparticulate mineralized collagen scaffolds via autogenous activation of the canonical BMP receptor signaling pathway. Biomaterials 2015; 50:107-114.
13. Ren X, Tu V, Bischoff D, et al. Nanoparticulate mineralized collagen scaffolds induce in vivo bone regeneration independent of progenitor cell loading or exogenous growth factor stimulation. Biomaterials 2016; 89:67-78.
14. Zhang Z, Li Z, Zhang C, et al. Biomimetic intrafibrillar mineralized collagen promotes bone regeneration via activation of the Wnt signaling pathway. International journal of nanomedicine 2018; 13:7503-7516.
15. Lee BL, Tang Z, Wang A, et al. Synovial stem cells and their responses to the porosity of microfibrous scaffold. Acta biomaterialia 2013; 9:7264-7275.
16. Bowers CA, McMullin JH, Brimley C, et al. Minimizing bone gaps when using custom pediatric cranial implants is associated with implant success. Journal of neurosurgery Pediatrics 2015; 16:439-444.
17. Tevlin R, McArdle A, Atashroo D, et al. Biomaterials for craniofacial bone engineering. Journal of dental research 2014; 93:1187-1195.
18. Hao Z, Song Z, Huang J, et al. The scaffold microenvironment for stem cell based bone tissue engineering. Biomater Sci 2017; 5:1382-1392.
19. Smith JO, Tayton ER, Khan F, et al. Large animal in vivo evaluation of a binary blend polymer scaffold for skeletal tissue-engineering strategies; translational issues. Journal of tissue engineering and regenerative medicine 2017; 11:1065-1076.
20. Mosher CZ, Spalazzi JP, and Lu HH. Stratified scaffold design for engineering composite tissues. Methods 2015; 84:99-102.

21. Wang DX, He Y, Bi L, et al. Enhancing the bioactivity of Poly(lactic-co-glycolic acid) scaffold with a nano-hydroxyapatite coating for the treatment of segmental bone defect in a rabbit model. International journal of nanomedicine 2013; 8:1855-1865.
22. Krampera M, Pizzolo G, Aprili G, et al. Mesenchymal stem cells for bone, cartilage, tendon and skeletal muscle repair. Bone 2006; 39:678-683.
23. BMP 2--Genetics Institute/ Medtronic-Sofamor Danek/Integra. Bone morphogenetic protein 2--Genetics Institute/ Medtronic-Sofamor Danek/Integra, INFUSE Bone Graft, recombinant human bone morphogenetic protein 2--Genetics Institute/Medtronic-Sofamor Danek/Integra, RhBMP 2--Genetics Institute/Medtronic-Sofamor Danek/Integra. BioDrugs. 2002;16(5):376-7. doi: 10.2165/00063030-200216050-00007. PMID: 12408742.
24. Ayoub A, Gillgrass T. The Clinical Application of Recombinant Human Bone Morphogenetic Protein 7 for Reconstruction of Alveolar Cleft: 10 Years' Follow-Up. J Oral Maxillofac Surg. 2019 Mar;77(3):571-581. doi: 10.1016/j.joms.2018.08.031. Epub 2018 Sep 5. PMID: 30273547.

CHAPTER 1: "Baseline model for bone regeneration"

Introduction

Reconstruction of mandibular bone defects following ablation or trauma of the head and neck is a surgical challenge. Bone-containing free tissue transfer (*e.g.*, scapular tip flap, fibular flap, iliac crest flap) [1–3] is generally preferred to bone grafting for many of these defects. However, such reconstructions are technically demanding, can lead to donor site morbidity and, moreover, they are burdened by failure or long bone repair times.

Bone tissue repair by using bioengineeered scaffolds may be considered an alternative approach and to this purpose different bio-scaffolds have been generated with the aim to favor the tissue bone regeneration.

Recently, we settled a novel and green synthetic strategy to produce a mechanically strong gelatin-based hydrogel using poly(ethylene glycol) diglycidyl ether as a cross-linker [4,5]. This hydrogel enriched with chitosan (HyCh) has been proven to be biocompatible, bioresorbable, sterilizable and suitable to support the hMSCs growth and their osteo-differentiation with mineralization [4, 6–8]. Furthermore, we also observed that the HyCh is able to trigger the osteogenic differentiation of hMSCs without external stimuli [9].

In addition to hydrogels alone, a three-dimensional integrated core-shell structure has been developed by grafting the softer bioactive HyCh-shell onto a stiffer thermoplastic porous core of poly(L-lactic acid)/poly(ε-caprolactone). The hybrid scaffolds, herein acronymized as PLA-PCL-HyCh, resulted in an exceptional improvement of mechanical properties compared to the pure hydrogel, closely mimicking both the stiffness and the morphology of bones. Furthermore, hybrid PLA-PCL-HyCh scaffolds showed excellent capability in supporting cell growth, osteogenic differentiation, and mineralization of bone marrow hMSCs (BM-hMSCs), demonstrating their potential application for bone regeneration [4–10].

A pilot translational study assessing bone regeneration sustained by HyCh and PLA-PCL-HyCh polymer scaffolds in an *in vivo* animal model is presented herein.

In this study, we tested the potential off the shelf HyCh and PLA-PCL-HyCh polymer bioengineered scaffolds in New Zealand rabbits for i) evaluating the *in vitro* and *in vivo* bone regenerative potential of materials developed by our research group (*i.e.*, HyCH and PLA-PCL-HyCh) [4,8,10]; ii) the safety of xenoimplantation of scaffolds seeded with human mesenchymal stromal cells (hMSC) in New Zealand rabbits; iii) investigating the effects of translationally relevant variables on the process of bone regeneration; iiii) analyzing the microarchitectural and immunohistochemical characteristics of new bone.

Materials and Methods

Study design

A preclinical study on an immunocompetent animal model (New Zealand rabbit, *Oryctolagus cuniculus*; body weight: 3 kg or higher) was designed to analyze the bone regenerative properties of bioengineered scaffolds (*i.e.*, HyCh and PLA-PCL-HyCh seeded with hMSCs) in non-critical-size mandibular defects.

Two study phases were planned: 1) an *in vitro* phase, that was aimed at verifying the presence of viable hMSCs in the scaffold at the time of surgery; 2) and an *in vivo* phase aimed at assessing the safety of the experimental procedure and evaluating the performance of bioengineered scaffold-based bone regeneration through multiple analyses (*i.e.*, *in vivo* and *ex vivo* radiological examinations and *ex vivo* histomorphological and immunohistochemical studies). Spontaneous bone regeneration has been studied as control (*i.e.*, considering animals with identical size of mandibular defects with either no reconstruction or unseeded scaffold-reconstruction"). The following variables were analyzed: 1) type of the scaffold (HyCh *vs* PLA-PCL-HyCh); 2) dimension of defect (3-5x3x3 mm^3 *vs* 15x3x3 mm^3); 3) type of contamination of the surgical site (sterile transcervical inferior mandibulectomy *vs* contaminated transoral teeth-sparing mandibulectomy); 4) quantity of seeded hMSCs (1000 cells/mm^3 *vs* 2000 cells/mm^3 *vs* 3000 cells/mm^3). The study workflow is summarized in **Figure 1**.

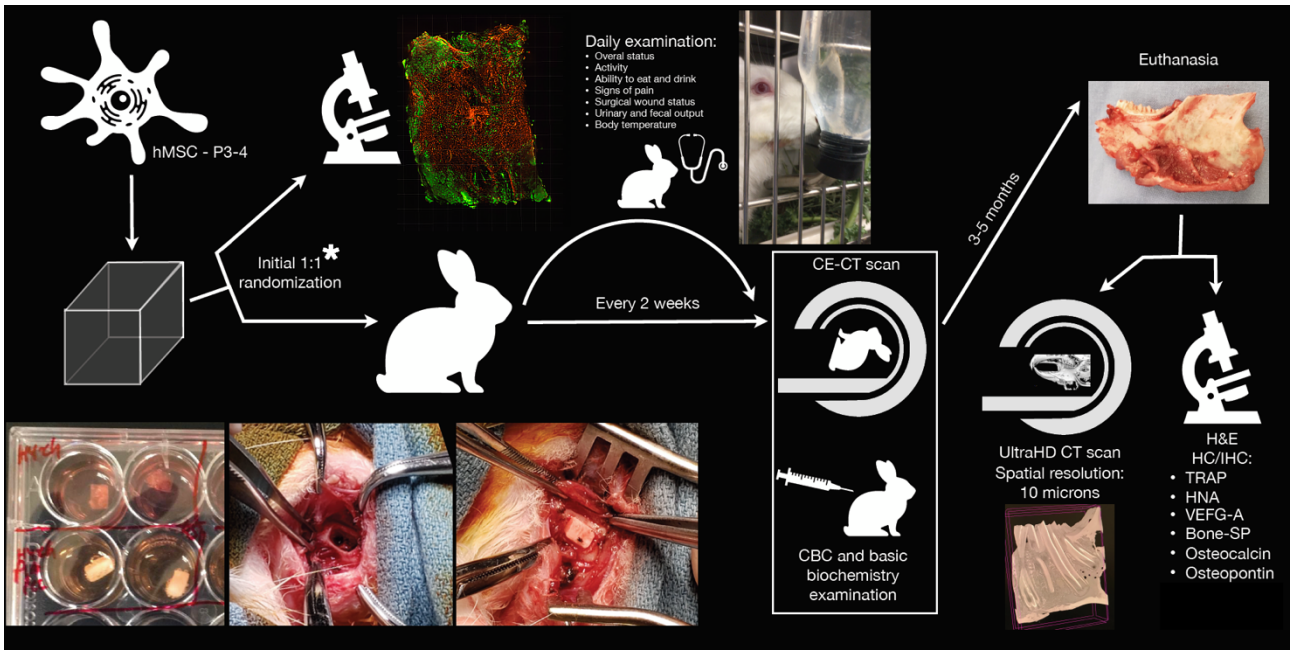

Figure 1. Schematic representation of the study workflow. *Randomization of two identical bioengineered scaffolds was performed to ascertain scaffolds were effectively seeded with viable human mesenchymal stromal cells (hMSCs) at the time of surgery. CBC, complete blood count; CE-CT, contrast-enhanced computed tomography; H&E, hematoxylin-eosin; HC/IHC, histochemistry/immunohistochemistry; HNA, human nuclear antigen; P3-4, passage 3-to-4; SP, sialoprotein; TRAP, tartrate-resistant acid phosphatase; UltraHD, ultra-high-definition; VEGF-A, vascular-endothelial growth factor-A.

Polymer scaffold synthesis

Two different biocompatible and bioresorbable polymeric scaffolds were tested: HyCh and PLA-PCL-HyCh.

HyCh is a highly porous and structurally stable hydrogel obtained by chemical crosslinking of poly (ethylene glycol) diglycidyl ether (PEG), gelatin (G), and chitosan (Ch). The material was prepared with a novel 2-step technique to increase the physical-mechanical stability of the scaffold: a first homogeneous phase reaction followed by freezing, freeze-drying, and a post-curing process. G, PEG and Ch content in the dry sample was 74.3%, 17.6%, and 8.1%, respectively [4].

An innovative synthetic approach was adopted to develop a hybrid core-shell scaffold with a PLA-PCL rigid core and HyCh soft shell. An interconnected porous core was safely obtained, avoiding solvents or other chemical issues, by blending PLA, PCL, and leachable superabsorbent polymer particles. After particle leaching in water, the resulting porous core was grafted with HyCh to create a bioactive shell within its pores. The final amount of grafted HyCh was 3% by weight [8,10]. **Figure 2** shows the morphological analysis of cryogenically obtained cross sections for HyCh and PLA-PCL-HyCh scaffolds. Both materials revealed a highly interconnected irregular open pore morphology which is conducive to the infiltration of cells.

Both dry scaffolds were packed in polypropylene bags and sterilized by gamma irradiation with cobalt 60 gamma rays (dose: 27-33 kGy, according to UNI EN ISO 11,137- Sterilization of Health Care Products) [11]. The scaffolds were developed and produced at the Department of Mechanical and Industrial Engineering, University of Brescia (Brescia, Italy) and then shipped to the Guided Therapeutics (GTx) Laboratory (University Health Network, University of Toronto, Toronto, ON, Canada).

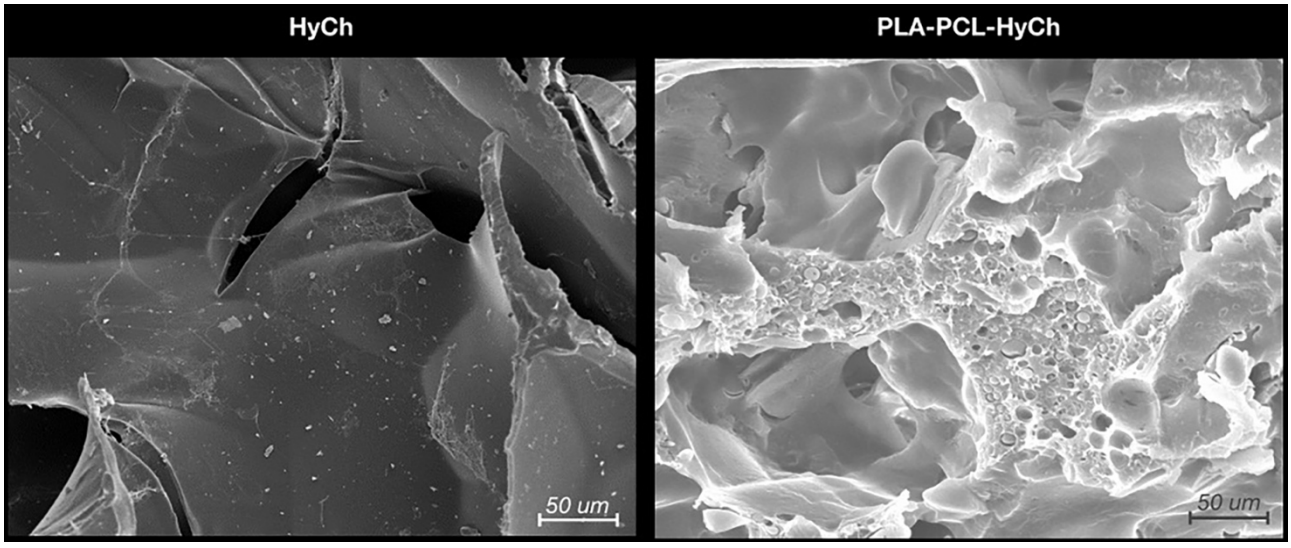

Figure 2. Microstructure of biomaterials (*i.e.*, hydrogel [HyCh] and the hybrid core-shell structure [PLA-PCL-HyCh]) as seen by scanning electron microscopy (SEM).

Human bone marrow mesenchymal stromal cell (hMSCs) culture

Human bone marrow hMSCs (BM-hMSCs) were harvested, isolated, and expanded to passage 3 or 4 (P3-4) before being used for the study; BM-hMSCs were donated from healthy consenting donors under an approved protocol in the Viswanathan Lab (Krembil Research Institute, University Health Network, University of Toronto, Toronto, ON, Canada). For hMSC expansion, 5% human platelet lysate (hPL, Stemcell Technologies), Dulbecco's Modified Eagle Medium (DMEM, Sigma Aldrich), a high glucose-based medium with 2% L glutamine/penicillin-streptomycin/amphotericin B solution (stock solution, 200 mM L-glutamine, 10,000 U/mL penicillin, 10 mg/mL streptomycin, 250 µg/mL amphotericin B), 1 mM sodium pyruvate, and MEM non-essential amino acids solution (1X) were employed.

In vitro and in vivo phases

Scaffolds were immersed in analogous growth medium seeded with hMSCs at different concentrations (1000, 2000, and 3000 cells/mm^3 of the scaffold volume); this was considered as time 0. The growth medium was renewed every 24 hours under sterile conditions. On day 4 (*i.e.*, 72 hours after seeding of scaffolds), the scaffolds were randomly divided into two groups (1:1 ratio), each undergoing a different experimental procedure, as follows:

1) *in vitro* cell viability assay: scaffolds were removed from the growth medium, stained with calcein (Invitrogen – Thermo Fisher Scientific; green, live cells) and propidium iodide (Bioshop; red, dead cells) following the manufacturer's instructions, and subsequently scanned with a 2-channel epifluorescence microscope (red, green) (AxioZoom microscope [Zeiss] with Plan NeoFluar Z 1X objective NA 0.25 and, an X-Cite 120 metal halide lamp). Images were acquired using a Hamamatsu ORCA Flash v2 sCMOS camera. Subsequently, images were deconvolved using Huygens Professional (Scientific Volume Imaging), and analyzed using Imaris (Bitplane Software, a Division of Oxford Imaging). This experiment aimed to demonstrate the presence of viable hMSCs in scaffolds at the time of surgery .

2) in vivo mandibular implantation in a rabbit model as detailed in the following sections.

*E*ighteen rabbits were used for the experimental study. Of these, 1 (5.6%) died in the early postoperative period (postoperative day [POD] 19), and thus 17 animals composed the study sample for measurements reported below. Overall, 24 surgical defects were created and 21 scaffolds implanted. **Table 1** summarizes surgical site distribution among study subgroups.

Study population	Site of the defect	Size of defect	Reconstruction strategy
17 rabbits (24 surgical implants)	Cervical (20)	Small (16) 5x3x3mm^3	No reconstruction (3)^{C1} HyCh (1)^{C2} PLA-PCL-HyCh (2)^{C2} HyCh + 1K-hMSCs (1) PLA-PCL-HyCh + 1K-hMSCs (1) HyCh + 2K-hMSCs (2) PLA-PCL-HyCh + 2K-hMSCs (2) HyCh + 3K-hMSCs (2) PLA-PCL-HyCh + 3K-hMSCs (2)
		Large (4) 15x3x3mm^3	HyCh + 2K-hMSCs (1) PLA-PCL-HyCh + 2K-hMSCs (1) HyCh + 3K-hMSCs (1) PLA-PCL-HyCh + 3K-hMSCs (1)
	Oral (4)	Small (4) 3x3x3 mm^3	HyCh + 2K-hMSCs (1) PLA-PCL-HyCh + 2K-hMSCs (1) HyCh + 3K-hMSCs (1) PLA-PCL-HyCh + 3K-hMSCs (1)

Table 1. Distribution of experimental reconstruction strategies employed in the study. Numbers in round parentheses refer to the number of surgical defects. C1, Controls with no reconstruction; C2, controls with unseeded scaffold-based reconstruction. (Legend: K= 1000).

Description of surgical procedures

Three different types of surgeries were performed on rabbits under general anesthesia with inhalant isoflurane (induction: 4 L/min; maintenance 1.5 L/min), after perioperative medication with antibiotic prophylaxis (intravenous cefazoline, 20 mg/kg) and analgesia (subcutaneous buprenorphine, 0.05 mg/kg) 30 minutes before surgery:

1) Bilateral inferior mandibulectomy (small defect): the inferior border of the mandible was exposed bilaterally through a 2-cm incision along the midline of the suprahyoid area. Periosteum and muscular insertions were dissected off the inferior aspect of the mandibular body and removed. Defects measuring 5x3x3 mm^3 (with 5 mm set along the greatest axis of the mandibular body) were drilled out at the inferior border of the mandible. After cauterizing the edges of the defect, scaffolds were positioned and secured by suturing a cuff of neighboring soft tissues. In control animals, bony defects were either filled with an unseeded scaffold or left unreconstructed. This procedure was performed on all animals included in 8 animals (**Figure 3**).
2) Unilateral inferior mandibulectomy (large defect): the inferior border of the mandible was exposed unilaterally through a 2-cm incision along the midline of the suprahyoid area. Defects measuring 15x3x3 mm^3 (with 15 mm set along the greatest axis of the mandibular body) were drilled out at the inferior border of the mandible. The scaffold was positioned and secured by suturing a cuff of neighboring soft tissues. This procedure was performed on 4 animals (**Figure 4A**).
3) Unilateral transoral teeth-sparing mandibulectomy (transoral defect): a horizontal, 1 cm long incision was made in the oral mucosa located between incisors and molars on one side. The mental nerve was identified and divided, and the respective bony foramen drilled to create a defect measuring 3x3x3 mm^3 at the superior border of mandible. After removing the adjacent periosteum, the scaffold was positioned and secured by suturing a cuff of neighboring soft tissues. This procedure was performed on 4 animals (**Figure 4B-D**).

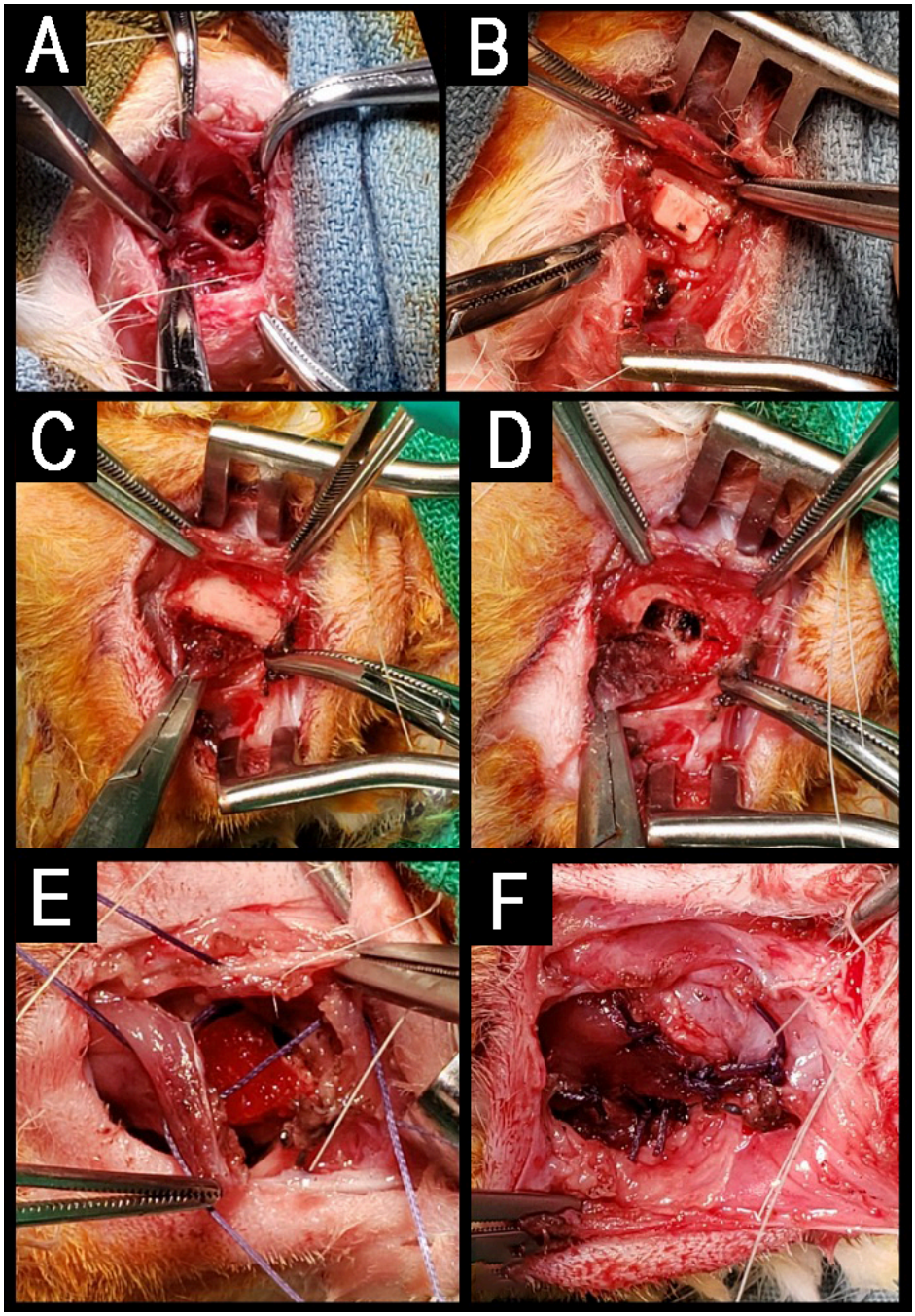

Figure 3. **A-B**. Inferior marginal mandibulectomy and positioning of a scaffold made of PLA-PCL-HyCh. **C-F**. Inferior marginal mandibulectomy and positioning of a scaffold made of HyCh, secured by suturing adjacent soft tissues.

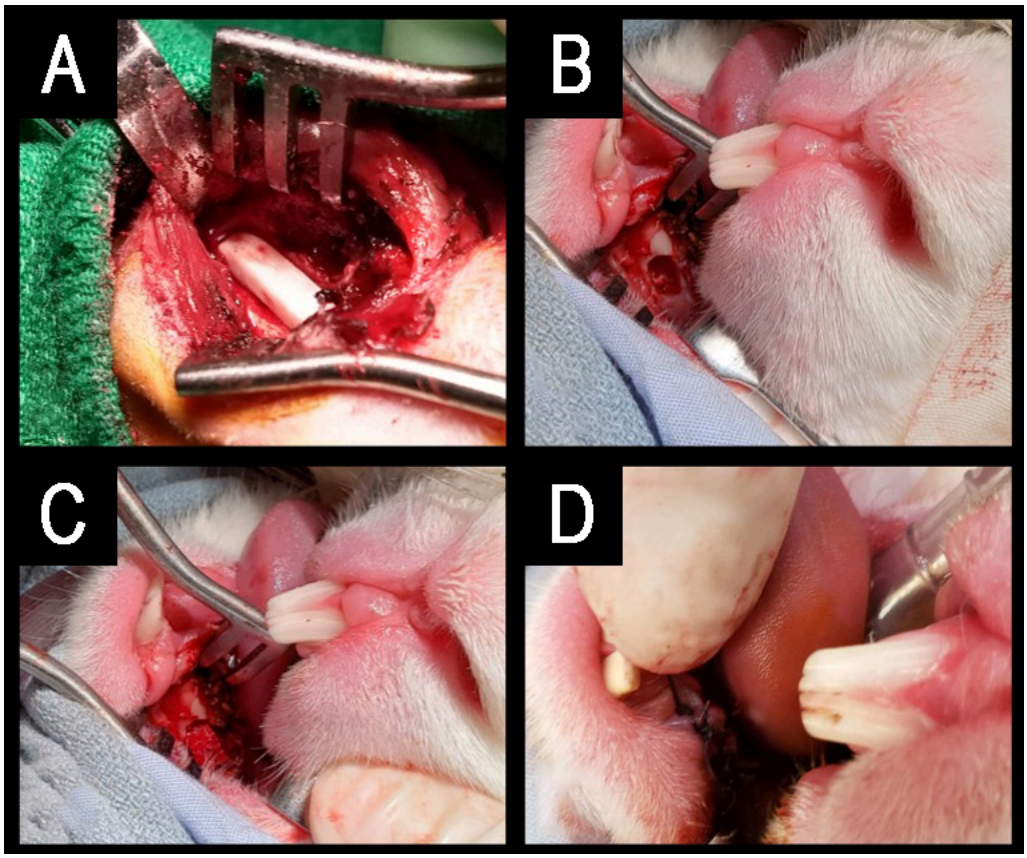

Figure 4. **A**. Inferior marginal mandibulectomy to create a large defect (15x3x3 mm^3) and positioning of a scaffold made of PLA-PCL-HyCh. **B-D**. Transoral teeth-sparing superior marginal mandibulectomy and positioning of a scaffold made of HyCh, secured by suturing the adjacent oral mucosa.

Animal monitoring and adverse events assessment

After surgery, animals were submitted to a daily clinical veterinary control, including evaluation of overall status, activity, feeding capacity, signs of pain, surgical wound status, urinary and fecal output, and body temperature. Weight was evaluated weekly, while biochemical monitoring with complete blood count (CBC) and basic biochemistry (renal and liver function) was performed every two weeks. For the first two weeks after surgery, soft food with appetizers was administrated to avoid excessive mechanical solicitation of the mandible.

According to the animal use protocol, in case of severe adverse events detected by the veterinary team, the animal might reach a humane endpoint, prompting the need of euthanasia. Humane endpoints were defined in case of persistent abnormal posture, untreatable anorexia and dehydration, persistent self-trauma, hemorrhagic discharge, and surgical site alterations compromising normal behavior, or causing dysphagia.

In vivo imaging acquisition and analysis

All rabbits underwent a CT scan (eXplore Locus Ultra MicroCT [General Electric, London, ON, Canada; voltage: 80 kV, current: 50 mA, isotropic voxel Size: 154 μm]) of the head and neck region before surgery. A biweekly radiological *in vivo* postoperative evaluation was also performed with the same scanner with and without contrast agent (Omnipaque iodine contrast agent [GE Healthcare, Chicago, IL, USA]). Imaging was acquired under general anesthesia with inhalant isoflurane (1.5 L/min).

The radiological images obtained were uploaded to 3D-modelling software (Mimics®/3-matic® Materialise®; research software license; Leuven, Belgium). The surgical site was identified and segmented in the first postoperative imaging. To ensure topographic consistency throughout measurements, each CT was co-registered to the first postoperative mandible and defect rendering. The average density at the implant site was measured in Hounsfield Units (HU) in the non-contrast-

enhanced (CE) acquisition. This value was defined as “absolute density”. The preoperative density at the implant site was considered as the complete restoration value (*i.e.*, 100% density restoration), while the first postoperative value acquired within 7-10 days after surgery was approximately defined as the baseline value (*i.e.*, 0% bone restoration). Thus, all absolute density measurements were rescaled and expressed as percentage, referred to as “relative density” (**Figure 5**).

The uptake of contrast medium at the surgical site, referred to as “uptake”, was measured as the difference between the average density in the CE acquisition minus the average density in the non-CE acquisition (**Figure 6A-B**).

The external surface of the defect (*i.e.*, the bone surface in contact with soft tissue) was segmented from the preoperative and postoperative CTs. A part-comparison-analysis between each postoperative segmentation and the respective preoperative one was performed [12–15]. Root mean square (RMS) of the part-comparison-analysis output was registered and used as an estimate of morphological similarity of the postoperative segmentations with respect to the preoperative one (*i.e.*, low root mean square indicates high morphological similarity) (**Figure 6C-D**).

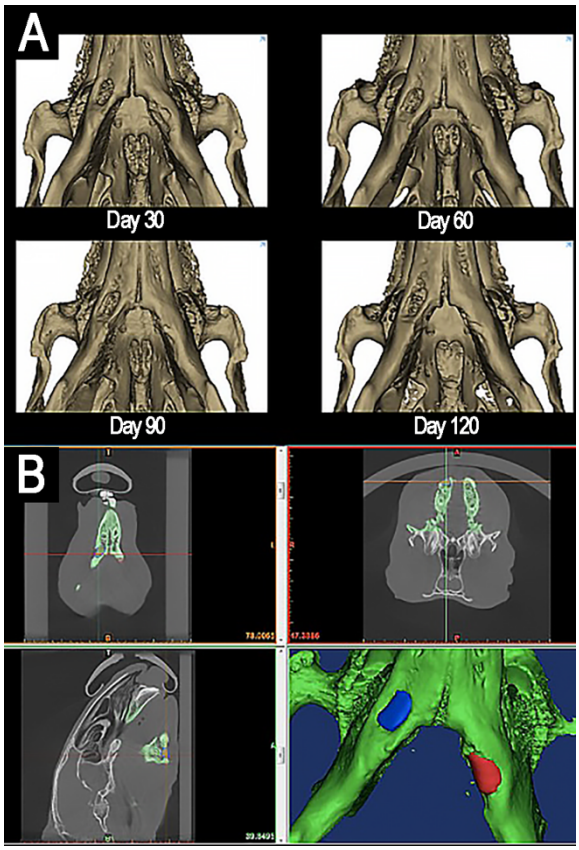

Figure 5. **A**. 3D-rendering of postoperative restoration of a bilateral defect of inferior marginal mandibulectomy, reconstructed with scaffolds made of PLA-PCL-HyCh on the right side and HyCh on the left side, at different timepoints. **B**. Methodology of measurement of the absolute density of the scaffolding area, identified and segmented in the first postoperative imaging.

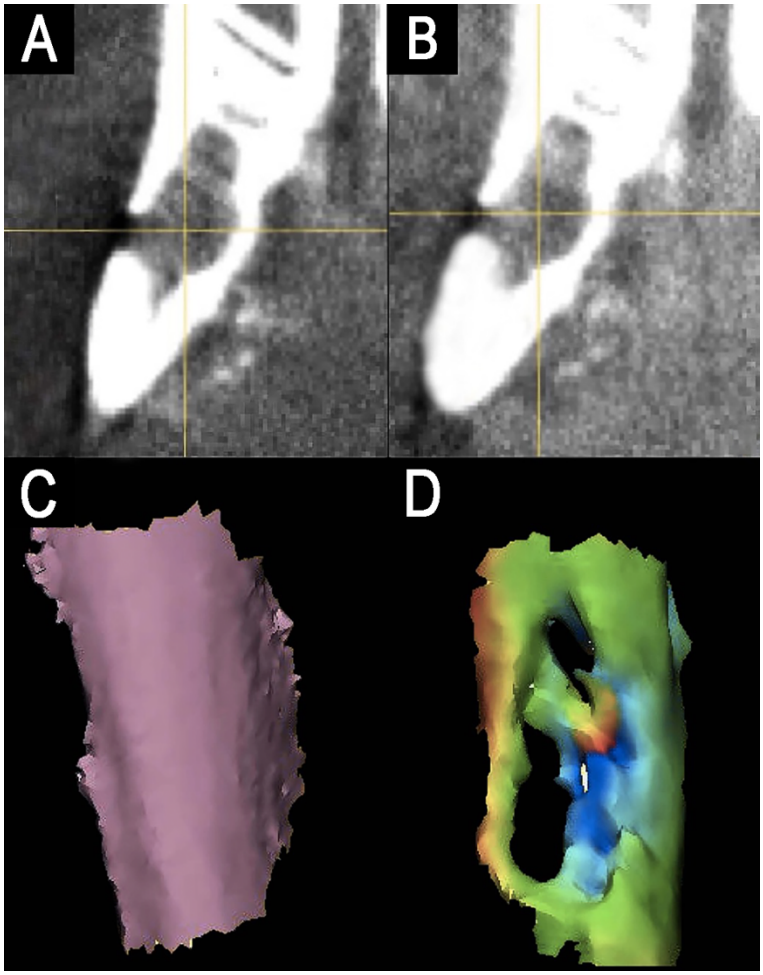

Figure 6. **A,B**. Pre- (A) and post-contrast (B) agent injection CT scan of the mandibular defect. Contrast enhancement can be appreciated in the defect area. **C,D**. Example of preoperative cortical shape (C) and 30-day postsurgical cortical shape (D) of the defect area. A color-scale map quantifies the morphological similarity between postsurgical and presurgical shapes (green areas are similar to the original shape, orange-to-red areas are excessively protruding with respect to the original shape, blue areas are depressed with respect to the preoperative shape).

Surgical endpoint

The scientific endpoint was set between 114 and 150 days from the surgical procedure. When the scientific endpoint was achieved, the animal was euthanized with an injection of 2.5 mL of potassium chloride (KCl) under general anesthesia obtained with inhalant isoflurane at 5% dosage. The mandible was then carefully removed, keeping the implant site protected and surrounded by a cuff of adjacent soft tissues.

Ex vivo imaging

The *ex vivo* radiological evaluation of the harvested specimens was performed by ultra-high-definition CT (SkyScan 1276 microCT system [Bruker, Belgium; voltage: 85 kV, current: 47 μA, isotropic voxel size: 10 μm]). On the images obtained, a region of interest (ROI) corresponding to the surgical defect repaired with the scaffold was manually identified through comparison with the first postoperative imaging (**Figure 7**). The software CT Analyser 1.17.7.2 (Bruker®) was used to extract quantitative data regarding the ROI (hereby referred to as "microarchitectural bone characteristics"), namely: 1) bone volume as percentage of the overall tissue volume; 2) mean trabecular thickness; 3) trabecular density per mm^3; and 4) mean trabecular separation in mm.

Sixteen ROIs were similarly analyzed in 4 rabbits (bilaterally, n=8) not included in the present study and in 8 rabbits included in the present study and receiving unilateral surgery on the mandibular body contralateral to the surgical site (n=8). The data extracted from this sample were used as an estimate of native bone microarchitectural bone characteristics.

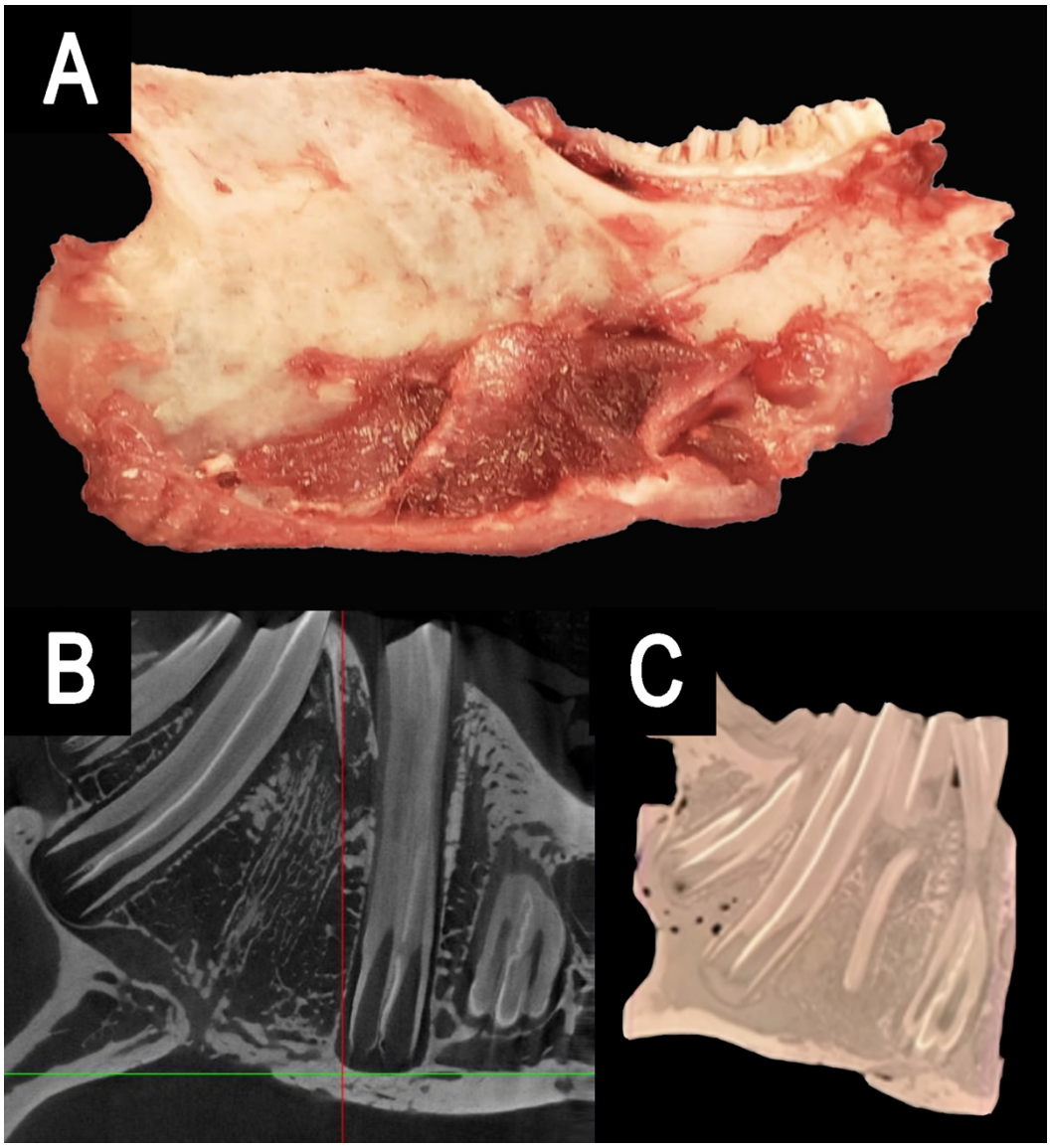

Figure 7. Ultra-high-definition CT on ex vivo specimens. **A**, The mandible is harvested after euthanasia. **B**, Cross-sectional 2D images on ultra-high-definition CT. **C**, Three-dimensional image reconstruction.

Specimen processing, staining, and histological imaging analysis

The surgical specimen, including the mandible and soft tissue surrounding the implanted sites, underwent a decalcification process with ethylenediaminetetraacetic acid (EDTA). Before paraffin embedding, each sample was cut at the level of scaffold's midpoint, obtaining two specimens to be subsequently processed with paracoronal histological slices (*i.e.*, with the cutting plane perpendicular to the greatest axis of the mandibular body). The site of the scaffold was identified by 3D-printing an actual-size mandibular model obtained from the first post-operative CT of each rabbit, thus comparing it to the harvested *ex vivo* mandibular specimen (3D Printer Dimension 1200es System Stratasys (Eden Prairie, MN, USA).

Histological sections were deparaffinized in xylene, rehydrated, and stained with H&E (Bio-Optica), to analyze general tissue morphology, and TRAP staining (Sigma-Aldrich, St. Louis, USA) to evaluate osteoclast activity, following the manufacturer's staining protocols. Histological slices underwent immunohistochemical staining with anti-VEGF-A (mouse monoclonal [VG-1], Abcam, Cambridge, UK; dilution: 1:500), anti-bone sialoprotein (mouse monoclonal [ID1.2], Immundiagnostik, Bensheim, Germany; dilution: 1:600), anti-osteocalcin (mouse monoclonal [OCG3], Genetex, Irvine, USA; dilution: 1:200), anti-osteopontin (mouse monoclonal [1B20], Novus Biologicals, Littleton, USA; dilution: 1:200), anti-human nuclear antigen antibodies (mouse monoclonal [235-1], Abcam, Cambridge, UK; dilution: 1:800).

The slides were digitalized with an Aperio AT2 brightfield scanner (Leica Biosystems, Concord, ON, Canada) and expression of the immunohistochemical markers within each considered ROI was quantitatively evaluated in terms of percentage of stain-positive area over total tissue area, using an image analysis platform for quantitative tissue analysis in digital pathology (Halo [Indica Lab, Albuquerque, NM, US]). The ROI was defined as the surface occupied by bony tissue in each slide, accounting for the area of the surgical defect. These data are referred to as "histological bone characteristics".

Statistical analysis

Statistical analysis was performed using RStudio (Version 1.2.5042). Two types of data were gathered for analysis: 1) time-dependent data and 2) endpoint data. The first cluster included relative density, uptake, and conformance restoration, whereas the second entailed microarchitectural bone characteristics and histological bone characteristics. These data were considered as the response variables and association thereof with the following explanatory variables was checked: scaffold employment (yes *vs* no), scaffold seeding (yes *vs* no *vs* no reconstruction), hMSC seeding concentration (1000 cells/mm^3 *vs* 2000 cells/mm^3 *vs* 3000 cells/mm^3 *vs* controls), defect site (oral *vs* cervical *vs* controls), defect size (small, including both 3x3x3 mm^3 and 5x3x3 mm^3 defects, *vs* large *vs* controls), material (HyCh *vs* PLA-PCL-HyCh *vs* no reconstruction), material and seeding status (unseeded HyCh *vs* HyCh+hMSC *vs* unseeded PLA-PCL-HyCh *vs* PLA-PCL-HyCh+hMSC *vs* no reconstruction).

Time-dependent data were modelled as linear models and graphically rendered through generalized additive model-generated regression lines on scatter plots. Time-dependent values were estimated through linear regression models at 60- and 120-day timepoints. Comparison between explanatory variable-determined subgroups was performed through analysis of variance with estimated marginal mean-based Tukey-adjusted *post hoc* test. For endpoint data, observations outlying the time interval between 120 and 150 days after surgery were considered as non-consistently comparable with other observations and were thus ignored (n=2: one animal was euthanized earlier than planned [POD 106] for COVID-19-pandemic-related logistical constraints; another animal was euthanized earlier than planned due to reaching a humane endpoint owing to pulmonary atelectasis [POD 71]). Endpoint data were graphically rendered through violin plots and analyzed through the Mann-Whitney test (for dichotomous explanatory variables) and the Kruskal-Wallis test (for non-dichotomous explanatory variables). Significance was set at 0.05 for all statistical

tests. P-values comprised between 0.05 (included) and 0.10 (excluded) were considered “close-to-significance”.

Ethics

The protocols (AUP#6010; title: *Primary reconstruction of maxillary and mandibular defects with computer-aided designing, computer-aided manufacturing bioengineered composite scaffolds*) for experimentation on animals were approved by the University Health Network Animal Care Committee (Princess Margaret Cancer Centre, University Health Network, University of Toronto) in April 2019.

Results

In vitro viability assay of bioengineered scaffolds

All (100%) randomly selected scaffolds showed viable cells (**Figure 8**) at the time of surgery (*i.e.* 72 hours after seeding of scaffolds). Mean cellular viability (viable cells/total cells) resulted 49.1% (range: 42.3-56.7%), and mean viable cells density 234 (range: 198-327) viable cells /mm^3.

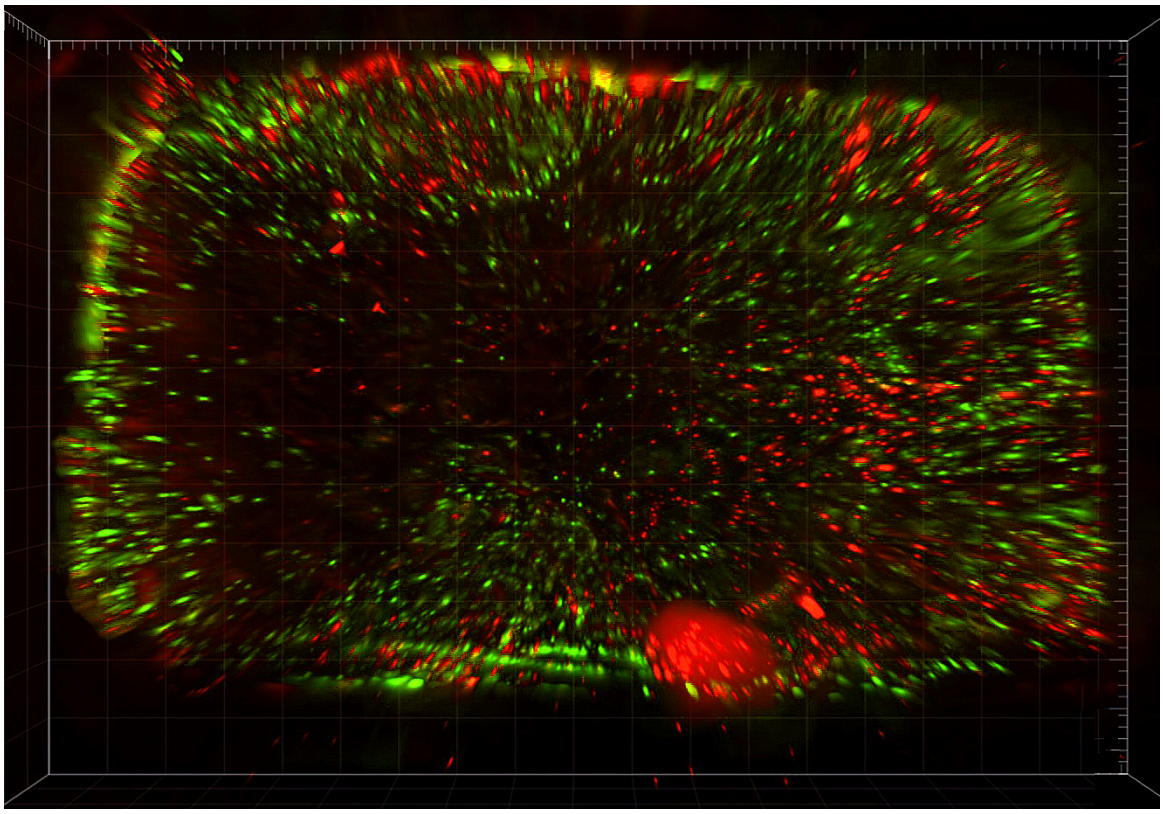

Figure 8. *In vitro* cell viability assay to assess and quantify the presence of vital cells: 3-dimensional rendering of an epifluorescence microscopy scanning of a scaffold seeded with human mesenchymal stem cells and stained with calcein and propidium iodide, which mark living and dead cells in green and red, respectively.

In vivo regenerative performance of bioengineered scaffolds

All animals showed a spontaneous trend of relative density increase (RDI) over time at the surgical site. RDI was significantly more pronounced in defects where a scaffold was placed as opposed to non-reconstructed sites (p=0.0018), particularly for scaffolds seeded with hMSCs (*vs* non-reconstructed sites p=0.0018; unseeded scaffolds *vs* non-reconstructed sites p=0.6459) (**Figure 9**;

Table 2). Overall, HyCh and PLA-PCL-HyCh did not show a significantly different RDI (p=0.2693), with both outperforming controls (p=0.0014 and p=0.0255, respectively). When considering the seeding status, seeded HyCh scaffolds showed the best performance in terms of RDI and they were the only subgroup with a statistically significant difference compared to non-reconstructed sites (p=0.0013). RDI of seeded PLA-PCL-HyCh scaffolds were close-to-significantly higher than that of non-reconstructed sites (p=0.0541).

Despite with no statistical significance (p=0.1212), non-reconstructed sites showed higher initial uptake with a decreasing trend over time, in contrast to scaffold-including sites, which displayed stable-to-mildly-increasing uptake over time. Addition of hMSCs to scaffolds created a small decrease in uptake, although with no significant difference (p=0.2930). Sites implanted with HyCh scaffolds as well as those with no reconstruction were significantly more permeable to the contrast agent than those with PLA-PCL-HyCh (p=0.0019 and p=0.0309, respectively). Both HyCh and PLA-PCL-HyCh scaffolds had a more stable uptake value over time when seeded with hMSCs, whereas controls showed a more variable trend.

Reduction of root mean square at part-comparison-analysis (RRP), which measures the similarity of the cortical bony contour of the surgical site compared to the preoperative shape, was greater in defects reconstructed with a scaffold, although with no statistical significance (p=0.7665).

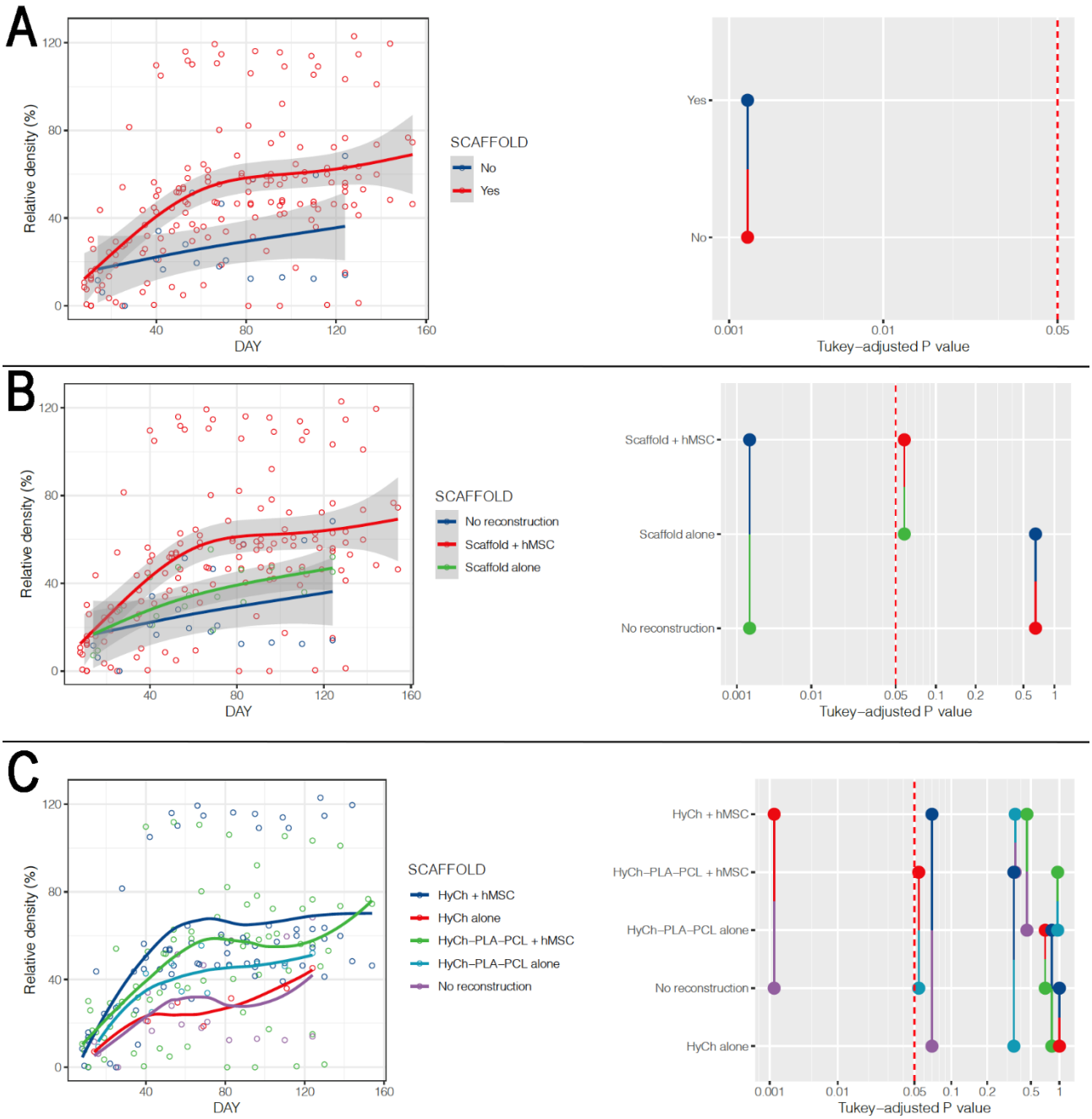

Figure 9. Relative density of the surgical site over time, stratified by presence or absence of the scaffold (A), employment of seeded vs unseeded scaffold (B), and according to seeding status and material composing the scaffold (C). Pairwise comparisons between categories and relative p-values are represented on the right of the figure.

Clustering variable	**60-day RD**	**120-day RD**	**p-value***
None (entire series)	42.7%	64.6%	N.A.
Scaffold (no *vs* yes)	No: 25.0% Yes: 44.8%	No: 40.1% Yes: 66.9%	**0.0018**
Scaffold type (no recon. *vs* HyCh *vs* PLA-PCL-HyCh)	No recon.: 25.0% HyCh: 47.8% PLA-PCL-HyCh: 42.0%	No recon.: 40.1% HyCh: 71.5% PLA-PCL-HyCh: 62.3%	**0.0023**
Scaffold seeding status (no recon. *vs* seeded scaffold *vs* unseeded scaffold)	No recon.: 25.0% Seeded scaffold: 46.4% Unseeded scaffold: 32.4%	No recon.: 40.1% Seeded scaffold: 68.7% Unseeded scaffold: 49.2%	**0.0006**
Scaffold type and seeding status (no recon. *vs* HyCh ± hMSCs *vs* PLA-PCL-HyCh ± hMSCs)	No recon.: 25.0% HyCh alone: 23.7% HyCh + hMSCs: 50.2% PLA-PCL-HyCh alone: 37.4% PLA-PCL-HyCh + hMSCs: 42.7%	No recon.: 40.1% HyCh alone: 41.6% HyCh + hMSCs: 74.1% PLA-PCL-HyCh: 54.9% PLA-PCL-HyCh + hMSCs: 63.2%	**0.0007**
Defect site (no seeding/no scaffold *vs* cervical *vs* oral)	No seeding/no scaffold: 28.7% Cervical: 43.7% Oral: 56.8%	No seeding/no scaffold: 44.6% Cervical: 64.3% Oral: 86.2%	**<0.0001**
Defect size (no seeding/no scaffold *vs* small *vs* large)	No seeding/no scaffold: 28.7% Small: 47.3% Large: 44.0%	No seeding/no scaffold: 44.6% Small: 71.9% Large: 60.8%	**0.0005**
hMSCs concentration (no cells *vs* 1000 cells/mm^3 *vs* 2000 cells/mm^3 *vs* 3000 cells/mm^3)	No seeding/no scaffold: 28.7% 1000 cells/mm^3: 41.4% 2000 cells/mm^3: 45.1% 3000 cells/mm^3: 49.4%	No seeding/no scaffold: 44.6% 1000 cells/mm^3: 61.9% 2000 cells/mm^3: 62.0% 3000 cells/mm^3: 78.1%	**0.0006**

Table 2. Estimates of relative density (RD) at 60 and 120 days after surgery, clustered by several explanatory variables considered in the study. *The p-value refers to the analysis of variance test (ANOVA) on linear regression models, see the text for relevant *post hoc* pairwise comparisons between categories. hMSC, human mesenchymal stromal cell; HyCh, hydrogel-chitosan scaffolds; PLA-PCL-HyCh, polylactic acid-polycaprolactone-hydrogel chitosan scaffolds.

Microarchitectural and histomorphological characteristics of new bone formation

Microarchitectural bone characteristics and their association with explanatory variables are summarized in **Table 3**. Native bone characteristics were significantly better (*i.e.*, higher relative bone volume, higher trabecular density, higher trabecular thickness, and lower intertrabecular distance) than regenerated bone, regardless the presence of a scaffold in the surgical site and seeding status (**Figure 10**).

On histomorphological analysis, all surgical sites showed mixed bone (*i.e.*, cortical and spongious). Use of a scaffold also affects the immunohistochemical profile of the regenerated bone (**Table 4**): 1) VEGF-A was significantly more expressed in defects reconstructed with a PLA-PCL-HyCh scaffold compared with HyCh ones and controls ($p=0.0123$); 2) Osteopontin was significantly more expressed in defects reconstructed with a scaffold than those left unreconstructed ($p=0.0332$) **(Figure 11)**.

Clustering variable	**Median percentage of bone (%)**	**Median trabecular thickness (mm)**	**Median trabecular density (mm^{-1})**	**Median trabecular separation (mm)**
None (entire series)	36.7	0.53	0.70	0.81
Scaffold	NB: 51.9 No: 27.0 Yes: 27.4 **p=0.0006**	NB: 0.84 No: 0.32 Yes: 0.30 **p=0.0002**	NB: 0.65 No: 0.86 Yes: 0.70 p=0.3907	NB: 0.68 No: 1.18 Yes: 1.00 p=0.0597
Scaffold type	NB: 51.9 NR: 27.0 Hy: 33.3 P: 19.3 **p=0.0017**	NB: 0.84 NR: 0.32 Hy: 0.31 P: 0.30 **p=0.0007**	NB: 0.65 NR: 0.86 Hy: 0.90 P: 0.51 p=0.0934	NB: 0.68 NR: 1.18 Hy: 0.76 P: 1.20 p=0.0797
Scaffold seeding status	NB: 51.9 NR: 27.0 Seeded: 31.0 Unseeded: 17.4 **p=0.0014**	NB: 0.84 NR: 0.32 Seeded: 0.32 Unseeded: 0.25 **p=0.0004**	NB: 0.65 NR: 0.86 Seeded: 0.70 Unseeded: 0.65 p=0.5897	NB: 0.68 NR: 1.18 Seeded: 1.00 Unseeded: 1.14 p=0.1284
Scaffold type and seeding status	NB: 51.9 NR: 27.0 Hy: 26.6 Hy+hMSCs: 33.9 P-Hy: 8.1 P-Hy+hMSCs: 21.4 **p=0.0069**	NB: 0.84 NR: 0.32 Hy: 0.28 Hy+hMSCs: 0.35 P-Hy: 0.22 P-Hy+hMSCs: 0.32 **p=0.0026**	NB: 0.65 NR: 0.86 Hy: 0.93 Hy+hMSCs: 0.82 P-Hy: 0.36 P-Hy+hMSCs: 0.58 p=0.1716	NB: 0.68 NR: 1.18 Hy: 0.67 Hy+hMSCs: 0.79 P-Hy: 1.61 P-Hy+hMSCs: 1.11 p=0.1486
Defect site	NB: 51.9 NSNS: 26.1 Cervical: 30.6 Oral: 30.7 **p=0.0014**	NB: 0.84 NSNS: 0.30 Cervical: 0.32 Oral: 0.28 **p=0.0005**	NB: 0.65 NSNS: 0.86 Cervical: 0.70 Oral: 0.81 p=0.8315	NB: 0.68 NSNS: 1.18 Cervical: 1.02 Oral: 0.71 p=0.0798
Defect size	NB: 51.9 NSNS: 26.1 Small: 35.6 Large: 18.4 **p=0.0004**	NB: 0.84 NSNS: 0.30 Small: 0.34 Large: 0.30 **p=0.0004**	NB: 0.65 NSNS: 0.86 Small: 0.72 Large: 0.55 p=0.4783	NB: 0.68 NSNS: 1.18 Small: 0.79 Large: 1.46 **p=0.0146**
hMSCs concentration	NB: 51.9 NSNS: 26.1 1K cells/mm^3: 31.8 2K cells/mm^3: 32.3 3K cells/mm^3: 26.3 **p=0.0028**	NB: 0.84 NSNS: 0.30 1K cells/mm^3: 0.45 2K cells/mm^3: 0.30 3K cells/mm^3: 0.33 **p=0.0013**	NB: 0.65 NSNS: 0.86 1K cells/mm^3: 0.70 2K cells/mm^3: 0.82 3K cells/mm^3: 0.60 p=0.8252	NB: 0.68 NSNS: 1.18 1K cells/mm^3: 1.00 2K cells/mm^3: 0.92 3K cells/mm^3: 0.98 p=0.2024

Table 3. Microarchitectural bone characteristics, clustered by several explanatory variables considered in the study. P-values refer to the Kruskal-Wallis test. 0-3K, 0/1000/2000/3000 cells/mm^3 at time of scaffold seeding; hMSC, human mesenchymal stromal cell; Hy, hydrogel-chitosan scaffolds; P, polylactic acid-polycaprolactone-hydrogel chitosan scaffolds; NB, native bone; NR, no reconstruction; NSNS, no seeding / no scaffold.

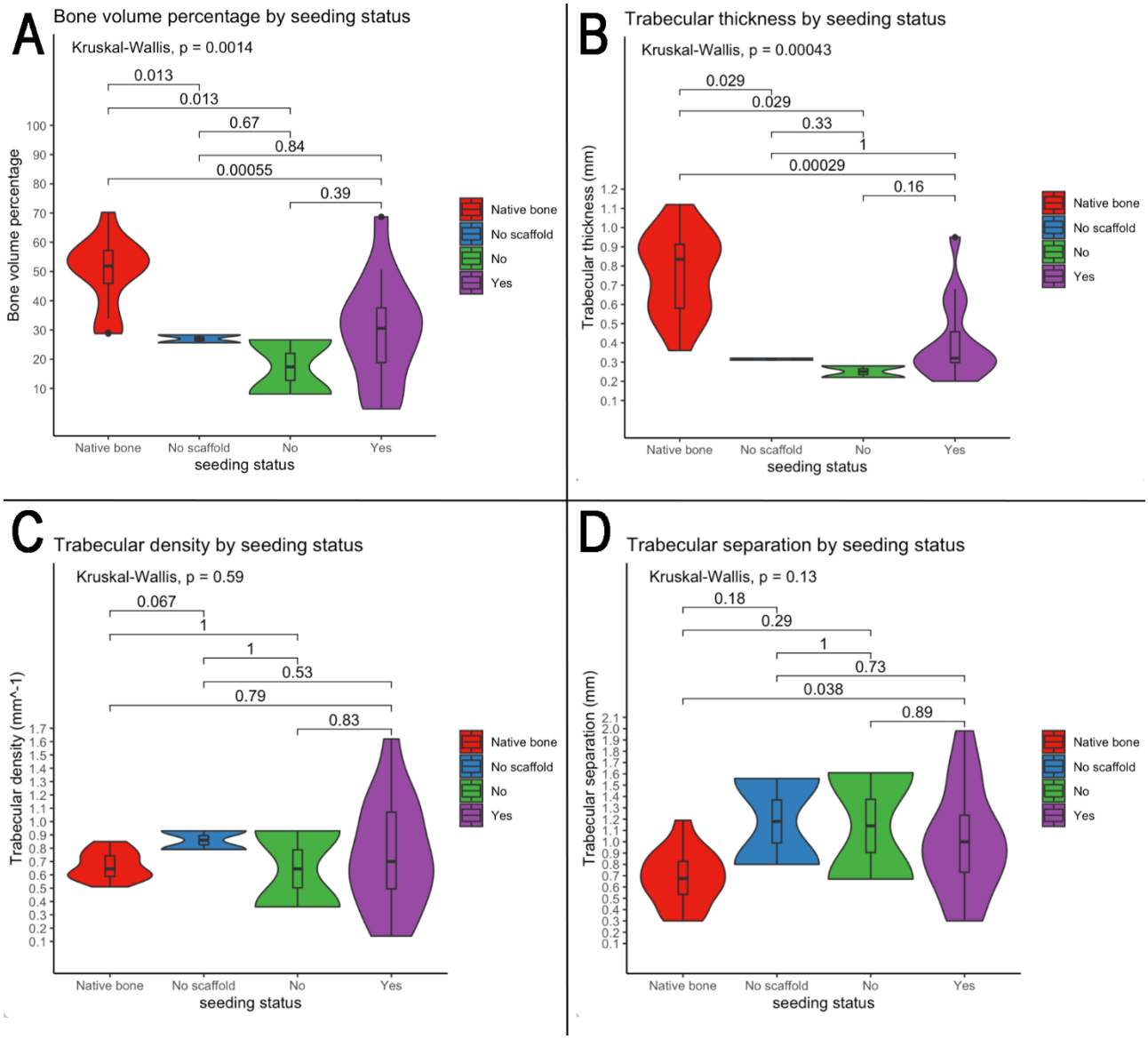

Figure 10. Violin plots showing that the microarchitectural characteristics of regenerated bone did not equate those of the native bone, irrespective of the employment of a scaffold and seeding with human mesenchymal stem cells. Of note, among study subgroups only the seeded scaffold included some cases equating to native bone in terms of bone volume and trabecular thickness.

Clustering variable	**HNA SA/TSA (%)**	**Osteocalcin SA/TSA (%)**	**Osteopontin SA/TSA (%)**	**Sialoprotein SA/TSA (%)**	**TRAP SA/TSA (%)**	**VEGF-A SA/TSA (%)**
Scaffold	No: 0.37 Yes: 1.03 p=0.0807	No: 22.50 Yes: 20.91 p=0.9337	No: 0.67 Yes: 6.05 **p=0.0332**	No: 0.98 Yes: 2.91 p=0.4739	No: 0.34 Yes: 0.23 p=0.8407	No: 0.21 Yes: 0.21 p=0.9062
Scaffold type	NR: 0.37 Hy: 1.39 P: 0.43 p=0.0709	NR: 22.95 Hy: 15.86 P: 22.70 p=0.5063	NR: 0.67 Hy: 7.18 P: 4.65 p=0.1004	NR: 0.98 Hy: 3.12 P: 2.77 p=0.7536	NR: 0.34 Hy: 0.38 P: 0.15 p=0.4385	NR: 0.21 Hy: 0.14 P: 0.32 **p=0.0123**
Scaffold seeding status	NR: 0.37 Seeded: 1.03 Unseeded: 0.76 p=0.2110	NR: 22.50 Seeded: 18.751 Unseeded: 28.345 p=0.6079	NR: 0.67 Seeded: 6.05 Unseeded: 7.03 p=0.0937	NR: 0.98 Seeded: 3.06 Unseeded: 0.17 p=0.2576	NR: 0.34 Seeded: 0.30 Unseeded: 0.20 p=0.9787	NR: 0.21 Seeded: 0.20 Unseeded: 0.27 p=0.7835
Defect site	NSNS: 0.37 Cervical: 1.03 Oral: 1.64 p=0.1925	NSNS: 22.50 Cervical: 22.70 Oral: 9.71 **p=0.0200**	NSNS: 0.67 Cervical: 9.83 Oral: 3.41 **p=0.0124**	NSNS: 0.98 Cervical: 1.86 Oral: 4.08 **p=0.0226**	NSNS: 0.34 Cervical: 0.23 Oral: 0.29 p=0.6988	NSNS: 0.21 Cervical: 0.21 Oral: 0.22 p=0.9557
Defect size	NSNS: 0.37 Small: 0.53 Large: 1.54 p=0.1620	NSNS: 22.50 Small: 21.65 Large: 15.33 p=0.5072	NSNS: 0.67 Small: 6.05 Large: 7.00 p=0.0991	NSNS: 0.98 Small: 3.09 Large: 2.41 p=0.7419	NSNS: 0.34% Small: 0.41 Large: 0.13 **p=0.0295**	NSNS: 0.21 Small: 0.21 Large: 0.13 p=0.4640
hMSCs concentration	0-1K cells/mm^3: 0.48 2-3K cells/mm^3: 1.33 **p=0.0433**	0-1K cells/mm^3: 22.60 2-3K cells/mm^3: 18.75 p=0.6408	0-1K cells/mm^3: 4.80 2-3K cells/mm^3: 5.96 p=0.4483	0-1K cells/mm^3: 0.91 2-3K cells/mm^3: 3.12 p=0.1185	0-1K cells/mm^3:0.42 2-3K cells/mm^3: 0.22 p=0.1904	0-1K cells/mm^3: 0.20 2-3K cells/mm^3: 0.21 p=0.4990

Table 4. Histological and immunohistochemical bone characteristics, clustered by explanatory variables considered in the study. P-values refer to the Kruskal-Wallis test. 0-3K, 0/1000/2000/3000 cells/mm^3 concentration at time of scaffold seeding; hMSC, human mesenchymal stromal cell; Hy, hydrogel-chitosan scaffolds; P, polylactic acid-polycaprolactone-hydrogel chitosan scaffolds; NB, native bone; NR, no reconstruction; NSNS, no seeding / no scaffold; SA, stained area; TSA, total selected area.

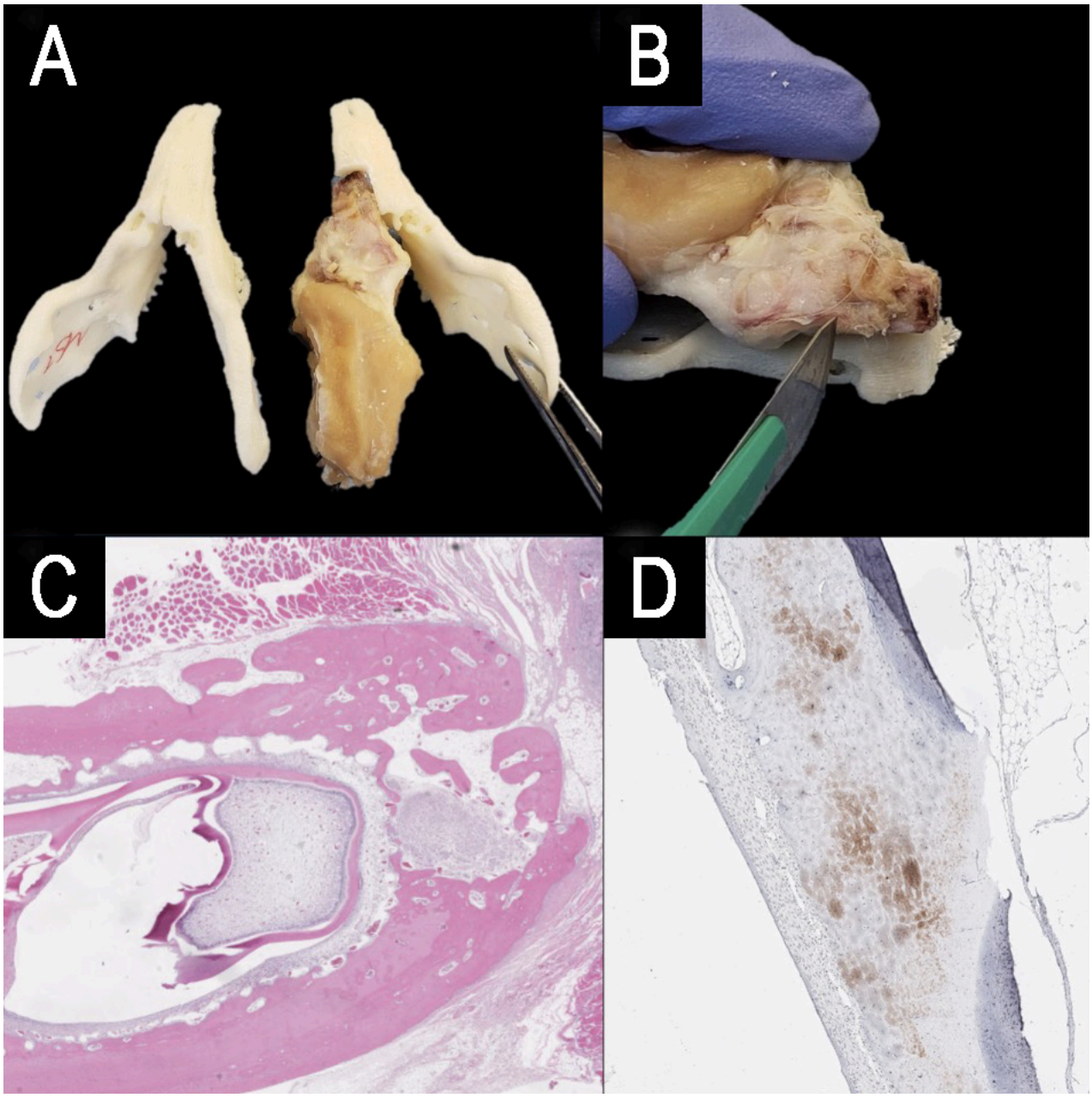

Figure 11. Steps of *ex vivo* specimen processing: production of a 3D printed model of each rabbit's mandible, based on the first postoperative CT, and checking the morphological fitting with the decalcified *ex vivo specimen* (A); matching the surgically treated area of the specimen with the corresponding site on the model, and cutting the specimen at the midpoint of the surgical defect area, to obtain the samples for histological analysis (B); hematoxylin-eosin staining (C); immunohistochemical staining (anti-HNA).

Effects of cell concentration at the time of seeding

Cell concentration at seeding also influenced RDI, with only 2000 and 3000 cells/mm^3 being associated with significantly higher RDI compared to controls (p=0.0144 and p=0.0002, respectively). RRP over time was significantly associated with hMSC concentration at seeding. In fact, 2000 and 3000 cells/mm^3 showed greater RRP than 1000 cells/mm^3 (p=0.0005 and p=0.0031, respectively). Human nuclear antigen was significantly more expressed in defects reconstructed through a scaffold seeded with 2000 and 3000 cells/mm^3 compared with 1000 cells/mm^3 and no seeding (p=0.0433).

Effects of defect size and type

There was no significant difference in terms of RDI relative to the size of the defect (small *vs* large p=0.6407), while both small and large defects showed higher RDI if reconstructed with seeded scaffolds in contrast to controls (p=0.0002 and p=0.0444, respectively). The size of the defect was associated with uptake trend over time, with only reconstructed large defects showing significantly lower uptake compared with controls (p=0.0205). TRAP stain was significantly associated with defect size, with large defects showing a lower staining value compared with small defects (p=0.0295).

Defects of the oral aspect of the mandible showed a higher RDI compared to those located on the cervical aspect (p=0.0213). Both sites showed a higher RDI if reconstructed with seeded scaffolds in contrast to controls (p<0.0001 and p=0.0042, respectively). Uptake of defects of the oral aspect of the mandible was similar and higher compared with non-reconstructed (p=0.8966) and reconstructed mandibular cervical sites (p=0.0048), respectively. Defects of the oral aspect of the mandible were associated with greater RRP than those created through the neck (p<0.0001). Bone sialoprotein was more expressed in defects of the oral aspect of the mandible (p=0.0226), and osteocalcin and osteopontin in those of the cervical surface of the mandible (p=0.0200 and p=0.0124, respectively).

Mortality and adverse events

Out of 18 rabbits initially included in the study, 1 died on POD 19, for a perioperative (*i.e.*, within 1 month) mortality of 5.3%. This animal developed an infectious pneumonia with atelectasis and was euthanized as the humane endpoint was deemed reached. Among the remaining 17 rabbits, one animal was found dead on POD 71 and the autopsy showed pulmonary hemorrhage, cardiomegaly, and coronary thrombosis. In neither of these two cases could a clear relationship with the experimental protocol be established.

All animals ate and showed regular urinary and fecal output within 48 hours from surgery. Serial peripheral blood examination did not show any clinically relevant variations in terms of hemoglobin, cell count (*i.e.*, erythrocytes, leukocytes, platelet), circulating leukocyte subpopulations, hepatic enzymes (*i.e.*, transaminases, gamma-glutamyl transferase), and creatinine.

No signs of surgical site infection were observed during the first 2 months after surgery. In 1/17 (5.9%) rabbit, the surgical site was swollen and reddened during the 3rd month after surgery. Since this alteration did not resolve with antibiotic therapy, the site was punctured, and 1 mL of purulent material was drained. After drainage, the surgical site recovered uneventfully.

Discussion

Bioengineered scaffolds outperformed the spontaneous bone regeneration process

The present study demonstrated that bone regeneration in the mandible is faster and more efficient when a scaffold composed of either HyCh or PLA-PCL-HyCh seeded with hMSCs is placed in the bony defect. In particular, HyCh with hMSCs was associated with the best performance, with density of the surgical site, measured with *in vivo* imaging, reaching roughly 50-to-70% of the native density at 2 to 4 months after surgery. PLA-PCL-HyCh with hMSCs also showed excellent performance, with roughly 40-60% of the native density being restored over the same time span. Of note, both these bioengineered materials outperformed controls with no reconstruction, where spontaneous bone regeneration took place. Interestingly, when focusing on unseeded scaffolds, only PLA-PCL-HyCh was associated with an improvement in terms of RDI, whereas HyCh showed a bone regeneration performance that was similar to non-reconstructed controls. This might be related to the intrinsic osteogenic properties of PLA-PCL in contrast to HyCh [16–18]. However, HyCh was associated with the highest enhancement of the surgical site in the long term, which is consistent with the belief that HyCh promotes neoangiogenesis. The molecular profile of newly formed bone also corroborated an active role played by scaffolds in the regeneration process. Osteopontin expression was higher in defects implanted with a scaffold. This sialoprotein not only is expressed in differentiated cells of the osteogenic lineage such as osteoblasts and osteocytes, but also is a marker for bone remodeling which is essential to new bone formation and maintenance of adequate bone quality [19]. VEGF-A was more expressed in PLA-PCL-HyCh-reconstructed defects than HyCh-reconstructed and not reconstructed ones. VEGF-A is expressed and secreted in response to poor tissue oxygenation, which depends upon vascularity [20]. The fact that HyCh-reconstructed sites were associated with the lowest expression of VEGF-A could mean that tissues within those surgical sites were adequately oxygenated and is consistent with the pro-angiogenetic properties of this material.

These results reinforced the belief that different properties of HyCh and PLA-PCL-HyCh should be exploited to optimize the functionality of a bioengineered, bone-regenerative medical device. Besides merging PLA-PCL and HyCh at a microstructural level, creation of composite scaffolds with hybrid macrostructure including a PLA-PCL-HyCh framework with interspersed pure HyCh areas is a step forward in bone regeneration.

There is significant proof that hMSCs play an essential role in the bone regeneration process observed, which is consistent with other observations [21-27]. The presence of hMSCs significantly increased relative density restoration, with seeding concentration of 3000 cells/mm^3 being associated with the best performance. Although no effect on enhancement could be demonstrated when considering seeded scaffolds altogether, a clear increase in surgical site enhancement was associated with the 3000 cells/mm^3 group. These findings are consistent with the well-known osteogenic potential and pro-angiogenetic effect of hMSCs and suggest that 3000 cells/mm^3 is the optimal concentration among those studied herein [28,29]. Interestingly, cells staining positive for the human nuclear antigen were observed in the surgical site several months after surgery and were found to be more frequent in the 2000 and 3000 cells/mm^3 group compared with controls and the 1000 cells/mm^3 group. No information on cell differentiation was gathered. Therefore, this observation mandates further investigation, but might confirm that hMSCs do not act as simple bystanders or initial triggers, but could have integrated in the host and possibly coordinated the regeneration process for a relatively long period.

Finally, it is worth specifying that timing and entity of density restoration is probably inappropriate for the purpose of translating these scaffolds to the clinical setting. Optimization of the regenerative performance is indeed paramount, and the results presented here will establish a baseline reference for future experiments from our collaborative research group. Other groups have adopted promising strategies including use of ossification-triggering factors (*e.g.*, bone morphogenic proteins, HMGB-1) [21–27,30] and co-culture of endothelial progenitors [31,32].

Analysis of translationally relevant variables showed favorable results

The first translationally relevant variable analyzed in the present study was defect size. Mandibular defects requiring reconstruction in humans are usually large and include several mandibular segments among symphysis, parasymphysis, body, and ramus. While there is no universally accepted cutoff to define critical size defects in the rabbit's mandible, the defects created in the present study can be considered non-critical in size, which means that this experimental defect is supposed to spontaneously heal over a given time. The standard defect in the inferior aspect of the mandible was bi-cortical, three-dimensional, and had a volume of 45 mm^3 and drilled bony surface of 33 mm^2 in the defect bed. Other authors described a critical size defect created through a bi-cortical circular trephine with 1 cm diameter, which, considering a mean mandibular body thickness of around 5-7 mm, has a volume of 393-550 mm^3 with a drilled bony surface of 157-220 mm^2 in the defect bed [33,34]. Defects labelled as "large" in the present study were 3 times as large as small ones (135 mm^3 *vs* 45 mm^3; drilled bony surface in the defect bed 63 mm^2 *vs* 33 mm^2), but still did not reach the critical size volume. Periosteal removal and cauterization of defect edges should also be considered as factors challenging bone regeneration [35]. Irrespective of the non-critical size of the defects studied herein, it should be noted that non-reconstructed defects did not heal completely over 4 months. Most importantly, the study groups of defects reconstructed with bioengineered scaffolds showed a faster and more efficient bone regeneration process. In addition to defect size, the segmental *vs* marginal nature of a mandibular defect is of utmost importance from a clinical perspective and can be studied in rabbits [36]. A segmental defect, indeed, implies that the mandible is discontinued, thus requiring that the reconstruction can substitute for the mechanical function of the bone over the healing period. This aspect was not investigated in the present study and will represent the object of future research from our groups. Of relevance, large defects did not show a significantly reduced RDI as compared to small defects. Of note, large defects showed reduced enhancement in the surgical site, particularly in the early postoperative period. TRAP was found to be less expressed in large defects. Besides marking osteoclasts, TRAP is expressed by other cells in bone regeneration (*e.g.*, TRAP+

mononuclear cells), whose presence is considered a hallmark of active bone regeneration via periosteum-derived cells recruitment [37]. Thus, slightly less efficient bone regeneration in large defects was unveiled through immunohistochemistry and contrast-enhanced imaging. These findings further underline that regenerative strategies oriented towards large bony defects should be sensitive to re-vascularization of the surgical site. This is emphasized by the observation by Chen *et al.* that co-culturing endothelial progenitors with mesenchymal stem cells, channeling the scaffold to promote neo-angiogenesis [31,38].

The second translationally relevant variable analyzed in the present study was the defect site. Mandibular defects are most often created through clean-contaminated fields, which means that the reconstruction is temporarily in contact with saliva and oral microbes and is thus partially contaminated. Also, orocutaneous fistula can occur during the postoperative period, thus leading saliva and microbes to the healing surgical site. In contrast to reconstruction with free tissue transfer, which, being vascularized, benefit from immune system defense, scaffolds are prone to potential microbic contamination, which represents a relevant concern and is partially responsible for preventing their translation into clinical practice. In the present study, defects created through a clean-contaminated field did not show a reduced performance of bone regeneration, nor did they show signs of infection in the postoperative period. However, defects on the oral aspect of the mandible showed higher RDI, enhancement, and bone sialoprotein expression and lower osteopontin and osteocalcin expression compared with other experimental subgroups. These findings are cautiously encouraging in a perspective of performing scaffold-based reconstruction of the mandible. Nonetheless, besides contamination occurring during surgery, the mucosal wound was closed at the end of the procedure, which means that the surgical site was no longer in contact with potential sources of contamination in the postoperative period. This issue will be assessed in future experiments in order to analyze the consequences of prolonged contact of the scaffold with saliva and oral microbes.

The third translationally relevant variable analyzed in the present study was shape restoration, which is of primary importance in the field of craniofacial reconstruction. This issue was assessed

through part-comparison analysis, a method quantifying the morphological similarity between 2 objects, which is best expressed by means of RMS (*i.e.*, the lower is RMS the higher is morphological similarity)[39]. By comparing the cortical surface of the healing surgical site with the native cortical bone throughout the course of the study, the timing and the contour of the shape restoration could be measured. Cortical shape restoration was significantly more pronounced in defects located on the oral aspect of the mandible, which were though the smallest of the series, and in cases with 2000-3000 cells/mm^3 at the time of seeding (13-19% RMS increase with respect to control groups). While firm conclusions cannot be made based on these preliminary results, scaffolds and hMSCs might have played a role in favoring shape restoration. This issue should be investigated in larger and morphologically more complex defects.

New Zealand rabbits were chosen for the experimental model as they are cost-effective large animals, adequate for testing the overmentioned translationally relevant variables. The regenerative approach could be applicable to other species (*e.g.* dog, pig, and sheep) for further preclinical analysis, and in the future could be tested in a clinical trial, assessing whether or not it is can provide bone augmentation in humans.

Microarchitectural bone features were not completely restored by any regeneration process

The microarchitectural features assessed in the present study included relative bone volume, trabecular thickness, trabecular density, and trabecular separation, which are all essentially associated with mechanical properties of the bone [40]. While trabecular density and separation were not significantly different when comparing the study subgroups with a group of non-operated rabbits, relative bone volume and trabecular thickness were significantly reduced in regenerated bone irrespective of the reconstructive strategy. Interestingly, the only measurements equating the native bone microarchitecture in terms of relative bone volume and trabecular thickness were in the group of rabbits receiving seeded scaffold-based reconstruction (**Figure 11**). These findings suggest that the majority of regenerated bone areas were biomechanically inferior to the native bone around 4

months after surgery. Although this does not necessarily mean that regenerated bone is biomechanically inadequate to sustain mandibular functions such as chewing, it is logical to assert that microarchitectural bone features should be an additional outcome to be considered in future optimization of our and other bone regenerative devices.

Safety assessment

Overall, the experimental procedure presented here, including the surgery, synthetic material implantation, and xenograft, were relatively safe. Mortality was 5.3% within 1 month from surgery, which compares favorably with other results (33.3%) reported for segmental defects in rabbit mandibles [41]. The only case of early death was observed in a rabbit secondary to pneumonia with atelectasis. No bronchial foreign body was found at autopsy, nor did the latest white blood cell count suggest systemic immune deficiency. Another rabbit was found dead in the cage 71 days after surgery. Autopsy showed pulmonary hemorrhage, cardiomegaly, and coronary thrombosis, which suggested an acute myocardial ischemia with heart failure. A clear relationship with the experimental procedure could not be established in either of these cases.

In terms of infection of the surgical site, only a late event was observed. A small abscess was found 3 months after surgery in a rabbit that underwent a large mandibulectomy. Despite the time passed from surgery, a potential role played by the scaffold in determining or facilitating the surgical site infection could not be excluded.

Strengths and limitations

The main strengths of the present study are the clear demonstration of the gain in regenerative performance when scaffold are seeded with hMSCs, and the assessment of translationally relevant aspects of the model used for bone regeneration in head and neck surgery (*i.e.* bone regeneration after a mandibulectomy with a transcervical or a transoral approach). However, the present study has some limitations that are not negligible. First, the pilot nature unavoidably limits the evidence ensued from

the present analysis: experiments should be reproduced in triplicates for each variable. Second, we have arbitrarily chosen that scientific endpoint was achieved when the RDI had reached a plateau, therefore no long term outcome data are available.

Conclusions

The present preclinical study demonstrated that bone regeneration in the rabbit mandible can be boosted by scaffold composed of either HyCh or PLA-PCL-HyCh seeded with hMSCs. Compared to spontaneous regeneration of bone, which led to approximately 40% restoration of the presurgical bone density in around 120 days, scaffold- and seeded scaffold-reconstruction increased this outcome to roughly 50% and 70%, respectively. HyCh was associated with increased enhancement of the surgical site over time, and PLA-PCL-HyCh with spontaneous osteogenic activity from the unseeded scaffold. Several results suggest a significant role of hMSCs, whose presence in the scaffold was associated with increased relative density, enhancement, and shape restoration, particularly at a concentration at the time of scaffold seeding of 2000-3000 cells/mm^3. Native microarchitectural characteristics were not demonstrated in any experimental group. Overall, the experimental procedure was safe and not associated with adverse events relatable to scaffolds or xenotransplantation.

References

[1] M.J. Gibber, J.B. Clain, A.S. Jacobson, D. Buchbinder, S. Scherl, J.P. Zevallos, S. Mehra, M.L. Urken, Subscapular system of flaps: An 8-year experience with 105 patients, Head Neck. 37 (2015) 1200–1206. https://doi.org/10.1002/HED.23738.

[2] C.G. Wallace, Y.M. Chang, C.Y. Tsai, F.C. Wei, Harnessing the potential of the free fibula osteoseptocutaneous flap in mandible reconstruction, Plast Reconstr Surg. 125 (2010) 305–314. https://doi.org/10.1097/PRS.0B013E3181C2BB9D.

[3] J.M. Blumberg, P. Walker, S. Johnson, B. Johnson, E. Yu, M. Lacasse, D.K. Lam, B. Rittenberg, C.M.K.L. Yao, D. Chepeha, J.R. Almeida, D.P. Goldstein, R. Gilbert, Mandibular reconstruction with the scapula tip free flap, Head Neck. 41 (2019) 2353–2358. https://doi.org/10.1002/hed.25702.

[4] K. Dey, S. Agnelli, F. Re, D. Russo, G. Lisignoli, C. Manferdini, S. Bernardi, E. Gabusi, L. Sartore, Rational Design and Development of Anisotropic and Mechanically Strong Gelatin-Based Stress Relaxing Hydrogels for Osteogenic/Chondrogenic Differentiation, Macromol Biosci. 19 (2019). https://doi.org/10.1002/MABI.201900099.

[5] K. Dey, E. Roca, G. Ramorino, L. Sartore, Progress in the mechanical modulation of cell functions in tissue engineering, Biomater Sci. 8 (2020) 7033–7081. https://doi.org/10.1039/D0BM01255F.

[6] F. Re, L. Sartore, E. Borsani, M. Ferroni, C. Baratto, A. Mahajneh, A. Smith, K. Dey, C. Almici, P. Guizzi, S. Bernardi, G. Faglia, F. Magni, D. Russo, Mineralization of 3D Osteogenic Model Based on Gelatin-Dextran Hybrid Hydrogel Scaffold Bioengineered with Mesenchymal Stromal Cells: A Multiparametric Evaluation, Materials (Basel). 14 (2021). https://doi.org/10.3390/MA14143852.

[7] K. Dey, S. Agnelli, L. Sartore, Dynamic freedom: substrate stress relaxation stimulates cell responses, Biomater Sci. 7 (2019) 836–842. https://doi.org/10.1039/C8BM01305E.

[8] F. Re, L. Sartore, V. Moulisova, M. Cantini, C. Almici, A. Bianchetti, C. Chinello, K. Dey, S. Agnelli, C. Manferdini, S. Bernardi, N.F. Lopomo, E. Sardini, E. Borsani, L.F. Rodella, F. Savoldi, C. Paganelli, P. Guizzi, G. Lisignoli, F. Magni, M. Salmeron-Sanchez, D. Russo, 3D gelatin-chitosan hybrid hydrogels combined with human platelet lysate highly support human mesenchymal stem cell proliferation and osteogenic differentiation, J Tissue Eng. 10 (2019). https://doi.org/10.1177/2041731419845852.

[9] S. Bernardi, F. Re, K. Bosio, K. Dey, C. Almici, M. Malagola, P. Guizzi, L. Sartore, D. Russo, Chitosan-Hydrogel Polymeric Scaffold Acts as an Independent Primary Inducer of Osteogenic Differentiation in Human Mesenchymal Stromal Cells, Materials (Basel). 13 (2020). https://doi.org/10.3390/MA13163546.

[10] L. Sartore, C. Pasini, S. Pandini, K. Dey, M. Ferrari, S. Taboni, H.H.L. Chan, J. Townson, S. Viswanathan, S. Mathews, R.W. Gilbert, J.C. Irish, F. Re, P. Nicolai, D. Russo, Hybrid Core-Shell Polymer Scaffold for Bone Tissue Regeneration, Int J Mol Sci. 23 (2022). https://doi.org/10.3390/IJMS23094533.

[11] ISO 11137-1:2006(en), Sterilization of health care products — Radiation — Part 1: Requirements for development, validation and routine control of a sterilization process for medical devices, (n.d.). https://www.iso.org/obp/ui/fr/#iso:std:iso:11137:-1:ed-1:v1:en (accessed October 9, 2022).

[12] N.A. Pagedar, R.W. Gilbert, H. Chan, M.J. Daly, J.C. Irish, J.H. Siewerdsen, Maxillary reconstruction using the scapular tip free flap: a radiologic comparison of 3D morphology, Head Neck. 34 (2012) 1377–1382. https://doi.org/10.1002/HED.21946.

[13] J.C. Davies, H.H.L. Chan, J.M. Bernstein, D.P. Goldstein, J.C. Irish, R.W. Gilbert, Orbital Floor Reconstruction: 3-Dimensional Analysis Shows Comparable Morphology of Scapular and Iliac Crest Bone Grafts, J Oral Maxillofac Surg. 76 (2018) 2011–2018. https://doi.org/10.1016/J.JOMS.2018.03.034.

[14] H.H.L. Chan, J.H. Siewerdsen, A. Vescan, M.J. Daly, E. Prisman, J.C. Irish, 3D Rapid Prototyping for Otolaryngology-Head and Neck Surgery: Applications in Image-Guidance, Surgical Simulation and Patient-Specific Modeling, PLoS One. 10 (2015). https://doi.org/10.1371/JOURNAL.PONE.0136370.
[15] H. Chan, R.W. Gilbert, N.A. Pagedar, M.J. Daly, J.C. Irish, J.H. Siewerdsen, A new method of morphological comparison for bony reconstructive surgery: maxillary reconstruction using scapular tip bone, Https://Doi.Org/10.1117/12.845603. 7625 (2010) 1046–1053. https://doi.org/10.1117/12.845603.
[16 S.H. Teoh, B.T. Goh, J. Lim, Three-Dimensional Printed Polycaprolactone Scaffolds for Bone Regeneration Success and Future Perspective, Tissue Eng Part A. 25 (2019) 931–935. https://doi.org/10.1089/TEN.TEA.2019.0102.
[17] G. Narayanan, V.N. Vernekar, E.L. Kuyinu, C.T. Laurencin, Poly (lactic acid)-based biomaterials for orthopaedic regenerative engineering, Adv Drug Deliv Rev. 107 (2016) 247–276. https://doi.org/10.1016/J.ADDR.2016.04.015.
[18] N.S. Hwang, S. Varghese, H.J. Lee, Z. Zhang, J. Elisseeff, Biomaterials directed in vivo osteogenic differentiation of mesenchymal cells derived from human embryonic stem cells, Tissue Eng Part A. 19 (2013) 1723–1732. https://doi.org/10.1089/TEN.TEA.2013.0064.
[19] B. Depalle, C.M. McGilvery, S. Nobakhti, N. Aldegaither, S.J. Shefelbine, A.E. Porter, Osteopontin regulates type I collagen fibril formation in bone tissue, Acta Biomater. 120 (2021) 194–202. https://doi.org/10.1016/J.ACTBIO.2020.04.040.
[20] K. Hu, B.R. Olsen, The roles of vascular endothelial growth factor in bone repair and regeneration, Bone. 91 (2016) 30–38. https://doi.org/10.1016/J.BONE.2016.06.013.
[21] A. Ho-Shui-Ling, J. Bolander, L.E. Rustom, A.W. Johnson, F.P. Luyten, C. Picart, Bone regeneration strategies: Engineered scaffolds, bioactive molecules and stem cells current stage and future perspectives, Biomaterials. 180 (2018) 143–162. https://doi.org/10.1016/J.BIOMATERIALS.2018.07.017.
[22] H.D. Kim, S. Amirthalingam, S.L. Kim, S.S. Lee, J. Rangasamy, N.S. Hwang, Biomimetic Materials and Fabrication Approaches for Bone Tissue Engineering, Adv Healthc Mater. 6 (2017). https://doi.org/10.1002/ADHM.201700612.
[23] S. Hosseinpour, M. Ghazizadeh Ahsaie, M. Rezai Rad, M. taghi Baghani, S.R. Motamedian, A. Khojasteh, Application of selected scaffolds for bone tissue engineering: a systematic review, Oral Maxillofac Surg. 21 (2017) 109–129. https://doi.org/10.1007/S10006-017-0608-3.
[24 A. Roffi, G.S. Krishnakumar, N. Gostynska, E. Kon, C. Candrian, G. Filardo, The Role of Three-Dimensional Scaffolds in Treating Long Bone Defects: Evidence from Preclinical and Clinical Literature-A Systematic Review, Biomed Res Int. 2017 (2017). https://doi.org/10.1155/2017/8074178.
[25] S.P. Pilipchuk, A.B. Plonka, A. Monje, A.D. Taut, A. Lanis, B. Kang, W. v. Giannobile, Tissue engineering for bone regeneration and osseointegration in the oral cavity, Dent Mater. 31 (2015) 317–338. https://doi.org/10.1016/J.DENTAL.2015.01.006.
[26] R. C, B. ML, Adipose mesenchymal stem cells in the field of bone tissue engineering, World J Stem Cells. 6 (2014) 144. https://doi.org/10.4252/WJSC.V6.I2.144.
[27] SR. Motamedian, S. Hosseinpour, MG. Ahsaie, A. Khojasteh, Smart scaffolds in bone tissue engineering: A systematic review of literature, World J Stem Cells. 7 (2015) 657. https://doi.org/10.4252/WJSC.V7.I3.657
[28] C. Ulpiano, C.L. da Silva, G.A. Monteiro, Mesenchymal Stromal Cells (MSCs): A Promising Tool for Cell-Based Angiogenic Therapy, Curr Gene Ther. 21 (2021) 382–405. https://doi.org/10.2174/1566523221666210917114353.
[29] M. Yang, H. Zhang, R. Gangolli, Advances of mesenchymal stem cells derived from bone marrow and dental tissue in craniofacial tissue engineering, Curr Stem Cell Res Ther. 9 (2014) 150–161. https://doi.org/10.2174/1574888X09666140213142258.

[30] A. Monir, T. Mukaibo, A.B.M. Abd El-Aal, T. Nodai, T. Munemasa, Y. Kondo, C. Masaki, M.A. El-Shair, K. Matsuo, R. Hosokawa, Local administration of HMGB-1 promotes bone regeneration on the critical-sized mandibular defects in rabbits, Sci Rep. 11 (2021) 8950. https://doi.org/10.1038/S41598-021-88195-7.
[31] L. Chen, J. Wu, C. Wu, F. Xing, L. Li, Z. He, K. Peng, Z. Xiang, Three-Dimensional Co-Culture of Peripheral Blood-Derived Mesenchymal Stem Cells and Endothelial Progenitor Cells for Bone Regeneration, J Biomed Nanotechnol. 15 (2019) 248–260. https://doi.org/10.1166/JBN.2019.2680.
[32] S. Shanbhag, N. Pandis, K. Mustafa, J.R. Nyengaard, A. Stavropoulos, Cell Cotransplantation Strategies for Vascularized Craniofacial Bone Tissue Engineering: A Systematic Review and Meta-Analysis of Preclinical In Vivo Studies, Tissue Eng Part B Rev. 23 (2017) 101–117. https://doi.org/10.1089/TEN.TEB.2016.0283.
[33] S. Young, A.G. Bashoura, T. Borden, L.S. Baggett, J.A. Jansen, M. Wong, A.G. Mikos, Development and characterization of a rabbit alveolar bone nonhealing defect model, J Biomed Mater Res A. 86 (2008) 182–194. https://doi.org/10.1002/JBM.A.31639.
[34] S.R. Shah, S. Young, J.L. Goldman, J.A. Jansen, M.E. Wong, A.G. Mikos, A composite critical-size rabbit mandibular defect for evaluation of craniofacial tissue regeneration, Nat Protoc. 11 (2016) 1989–2009. https://doi.org/10.1038/NPROT.2016.122.
[35] P.L. Carlisle, T. Guda, D.T. Silliman, R.G. Hale, P.R.B. Baer, Are critical size bone notch defects possible in the rabbit mandible?, J Korean Assoc Oral Maxillofac Surg. 45 (2019) 97–107. https://doi.org/10.5125/JKAOMS.2019.45.2.97.
[36] M. Hirota, T. Shima, I. Sato, T. Ozawa, T. Iwai, A. Ametani, M. Sato, Y. Noishiki, T. Ogawa, T. Hayakawa, I. Tohnai, Development of a biointegrated mandibular reconstruction device consisting of bone compatible titanium fiber mesh scaffold, Biomaterials. 75 (2016) 223–236. https://doi.org/10.1016/J.BIOMATERIALS.2015.09.034.
[37] B. Gao, R. Deng, Y. Chai, H. Chen, B. Hu, X. Wang, S. Zhu, Y. Cao, S. Ni, M. Wan, L. Yang, Z. Luo, X. Cao, Macrophage-lineage TRAP+ cells recruit periosteum-derived cells for periosteal osteogenesis and regeneration, J Clin Invest. 129 (2019) 2578–2594. https://doi.org/10.1172/JCI98857.
[38] L. Vidal, M. Brennan, S. Krissian, J. de Lima, A. Hoornaert, P. Rosset, B.H. Fellah, P. Layrolle, In situ production of pre-vascularized synthetic bone grafts for regenerating critical-sized defects in rabbits, Acta Biomater. 114 (2020) 384–394. https://doi.org/10.1016/J.ACTBIO.2020.07.030.
[39] N.A. Pagedar, R.W. Gilbert, H. Chan, M.J. Daly, J.C. Irish, J.H. Siewerdsen, Maxillary reconstruction using the scapular tip free flap: a radiologic comparison of 3D morphology, Head Neck. 34 (2012) 1377–1382. https://doi.org/10.1002/HED.21946.
[40] E. Mittra, C. Rubin, Y.X. Qin, Interrelationship of trabecular mechanical and microstructural properties in sheep trabecular bone, J Biomech. 38 (2005) 1229–1237. https://doi.org/10.1016/J.JBIOMECH.2004.06.007.
[41] C.D. Lopez, J.R. Diaz-Siso, L. Witek, J.M. Bekisz, B.N. Cronstein, A. Torroni, R.L. Flores, E.D. Rodriguez, P.G. Coelho, Three dimensionally printed bioactive ceramic scaffold osseoconduction across critical-sized mandibular defects, J Surg Res. 223 (2018) 115–122. https://doi.org/10.1016/J.JSS.2017.10.027.

CHAPTER 2: "Optimization models for bone regeneration"

Introduction

In our pilot preclinical study (Chapter 1), we demonstrated that bone regeneration in the rabbit mandible can be boosted by scaffold composed of either HyCh or PLA-PCL-HyCh seeded with hMSCs. Compared to spontaneous regeneration of bone, which led to approximately 40% restoration of the presurgical bone density in around 90-120 days, scaffold- and seeded scaffold-reconstruction increased this outcome to roughly 50% and 70%, respectively. The experimental procedure resulted safe and not associated with adverse events relatable to scaffolds or xenotransplantation, but the regenerative performance needed to be optimized. The regenerative model must be remodulated to obtain a higher quantity of regenerated bone in a shorter period of time.

In literature there is a plenty of options available for each "ingredient" of the regenerative triad (*i.e.* scaffold, cells, and stimulating factor), and the real challenge is to find the winning combination[1].

Bone marrow-derived mesenchymal stromal cells (MSCs) are increasingly used for craniofacial defect repair, and several studies have substantiated their effectiveness as osteoblastic precursors in critical-sized defect reconstruction;[1–3] also, some authors believe that the allograft transplantation of MSCs is more efficient than the xenograft model, therefore rabbit MSCs (rMSCs) should be associate with a better regenerative performance in rabbit model.[4–6]

Bone morphogenic proteins (BMPs), members of the TGF-b family, have been used clinically to induce bone regeneration in critical-sized craniofacial defects as well as alveolar ridge and sinus augumentation.[7,8] Particularly BMP-2 and BMP-7 have been studied extensively in bone healing and produce superior fusion rates with fewer complications than autologous bone grafts.[9–16] Infuse Bone Graft (Medtronic and Wyeth) and Osigraft (Stryker Biotech) are two FDA-approved collagen-based scaffolds containing recombinant BMP-2 and BMP-7, respectively. The clinical success of these products demonstrates the importance of growth factors in osteogenesis and underscores the potential of growth factor-infused scaffolds.

We attempted to explore the possibility to optimize our baseline model testing the following strategies:

- Seeding scaffolds with rabbit mesenchymal stromal cells (rMSCs), addressing if an allograft model could be better than a xenograft one.
- Adding the growth factor BMP-2 to the baseline model (scaffold + hMSCs; Chapter 1).

Collaterally the ancillary aim of the present chapter was also to assess the possibility of obtain bone formation through the implantation of the baseline model (scaffold + hMSCs) in the subcutis, where the growth factor BMP-2 was also administrated.

Materials and Method

Study design (Subchapter 2.1): Rabbit mesenchymal stromal cells (rMSCs)

A preclinical study on an immunocompetent animal model (New Zealand rabbit, *Oryctolagus cuniculus*; body weight: 3 kg or higher) was designed to analyze the bone regenerative properties of bioengineered scaffolds (*i.e.*, HyCh and PLA-PCL-HyCh seeded with rMSCs) in non-critical-size mandibular defects.

Four rabbits were operated with bilateral inferior mandibulectomy (8 surgical defects), distribution of experimental reconstruction strategies (material and cell concentration) employed in the study are summarized in Table 1.

An in vivo phase aimed at assessing the safety of the experimental procedure and evaluating the performance of bioengineered scaffold-based bone regeneration through multiple analyses (*i.e.* in vivo and ex vivo radiological examinations and ex vivo histomorphological study). The following variables were analyzed: 1) type of the scaffold (HyCh vs PLA-PCL-HyCh); 2) quantity of seeded rMSCs (1000 cells/mm3 vs 2000 cells/mm3 vs 3000 cells/mm3). Subsequently the rabbits underwent the identical follow up protocol used for the baseline model (Chapter 1), with a biweekly radiological in vivo postoperative evaluation was also performed with CT scan with and without contrast agent. Imaging was acquired under general anesthesia with inhalant isoflurane (1.5 L/min).

Scaffold Material and cell concentration
Rabbit 1:
- *Right side: 1 HyCH + 1K cells/mm3*
- *Left side: 1 HyCH + 2K cells/mm3*
Rabbit 2:
- *Right side: 1 HyCH + 3k cells/mm3*
- *Left side: 1 PLA-PCL-HyCH + 1K cells/mm3*
Rabbit 3:
- *Right side: 1 PLA-PCL-HyCH + 2K cells/mm3*
- *Left side: 1 PLA-PCL-HyCH + 3K cells/mm3*
Rabbit 4:
- *Right side: 1 HyCH + 2K cells/mm3*
- *Left side: 1 PLA-PCL-HyCH + 3K cells/mm3*

Table 1 Distribution of experimental reconstruction strategies (material and cell concentration) employed in the study.

<u>*Study design (Subchapter 2.2): Bone morphogenetic protein 2 (BMP-2)*</u>

A preclinical study on an immunocompetent animal model (New Zealand rabbit, *Oryctolagus cuniculus*; body weight: 3 kg or higher) was designed to analyze the bone regenerative properties of bioengineered scaffolds (*i.e.*, HyCh seeded with hMSCs) in non-critical-size mandibular defects with the local injection of BMP-2 (1.25 μg a week for 4 weeks, reaching a total dose of 5 μg), performed through the ultrasound (US) guidance.

Three rabbits were operated with bilateral inferior mandibulectomy (6 surgical defects), and reconstruction was performed by an HyCH scaffold seeded with 2K cells/mm3 concentration of hMSCs in 5 cases, and by an unseeded HyCH scaffold in the remaining case.

An in vivo phase aimed at assessing the safety of the experimental procedure and evaluating the performance of bioengineered scaffold-based bone regeneration through multiple analyses (*i.e.* in vivo and ex vivo radiological examinations and ex vivo histomorphological study). Subsequently the rabbits underwent the identical follow up protocol used for the baseline model (Chapter 1) and for the rMSCs experiment (Subchapter 2.1).

Study design (Subchapter 2.3): Heterotopic bone formation

A preclinical study on an immunocompetent animal model (New Zealand rabbit, *Oryctolagus cuniculus*; body weight: 3 kg or higher) was designed to analyze the bone regenerative properties of bioengineered scaffolds (*i.e.*, HyCh seeded with hMSCs at the concentration of 2000 cells/mm^3) in the subcutis defects with the local injection of BMP-2 (1.25 μg a week for 4 weeks, reaching a total dose of 5 μg), performed through the ultrasound (US) guidance.

Three rabbits were operated with subcutaneous implantation (3 surgical defects at level of the rabbit dorsum) of an HyCH scaffold seeded with 2K cells/mm3 concentration of hMSCs in all cases.

An *in vivo* phase aimed at assessing the safety of the experimental procedure and evaluating the performance of bioengineered scaffold-based bone regeneration through multiple analyses (*i.e. in vivo* and *ex vivo* radiological examinations and *ex vivo* histomorphological study). Subsequently the rabbits underwent the identical follow up, applied in Chapter 1, with a biweekly radiological in vivo postoperative evaluation was also performed with US and CT scan with and without contrast agent. Imaging was acquired under general anesthesia with inhalant isoflurane (1.5 L/min).

Description of surgical procedures

Bilateral inferior mandibulectomies (small defect 5x3x3 mm; see Chapter 1 for more details) were performed on rabbits under general anesthesia with inhalant isoflurane (induction: 4 L/min; maintenance 1.5 L/min), after perioperative medication with antibiotic prophylaxis (intravenous cefazoline, 20 mg/kg) and analgesia (subcutaneous buprenorphine, 0.05 mg/kg) 30 minutes before surgery.

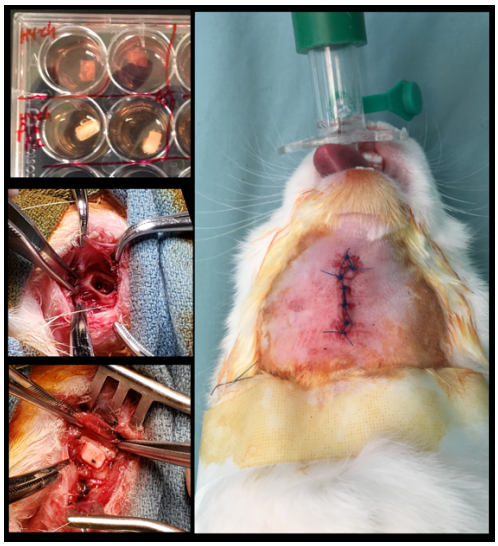

Figure 1 Inferior marginal mandibulectomy and positioning of a scaffold made of PLA-PCL-HyCh, secured by suturing adjacent soft tissues.

Subcutaneous implants were performed on rabbits under general anesthesia with inhalant isoflurane (induction: 4 L/min; maintenance 1.5 L/min), after perioperative medication with antibiotic prophylaxis (intravenous cefazoline, 20 mg/kg) and analgesia (subcutaneous buprenorphine, 0.05 mg/kg) 30 minutes before surgery (Figure 2).

Figure 2 Surgical site on the back of the rabbit prepared for the subcutaneous implantation.

Animal monitoring and adverse events assessment

After surgery, animals were submitted to a daily clinical veterinary control, including evaluation of overall status, activity, feeding capacity, signs of pain, surgical wound status, urinary and fecal output, and body temperature. Weight was evaluated weekly, while biochemical monitoring with complete blood count (CBC) and basic biochemistry (renal and liver function) was performed

every two weeks. For the first two weeks after surgery, soft food with appetizers was administrated to avoid excessive mechanical solicitation of the mandible.

According to the animal use protocol, in case of severe adverse events detected by the veterinary team, the animal might reach a humane endpoint, prompting the need of euthanasia. Humane endpoints were defined in case of persistent abnormal posture, untreatable anorexia and dehydration, persistent self-trauma, hemorrhagic discharge, and surgical site alterations compromising normal behavior, or causing dysphagia.

In vivo imaging acquisition and analysis

All rabbits underwent a CT scan (eXplore Locus Ultra MicroCT [General Electric, London, ON, Canada; voltage: 80 kV, current: 50 mA, isotropic voxel Size: 154 μm]) of the head and neck region before surgery. A biweekly radiological *in vivo* postoperative evaluation was also performed with the same scanner with and without contrast agent (Omnipaque iodine contrast agent [GE Healthcare, Chicago, IL, USA]). Imaging was acquired under general anesthesia with inhalant isoflurane (1.5 L/min).

The radiological images obtained were uploaded to 3D-modelling software (Mimics®/3-matic® Materialise®; research software license; Leuven, Belgium). The surgical site was identified and segmented in the first postoperative imaging. To ensure topographic consistency throughout measurements, each CT was co-registered to the first postoperative mandible and defect rendering. The average density at the implant site was measured in Hounsfield Units (HU) in the non-contrast-enhanced (CE) acquisition. This value was defined as "absolute density". The preoperative density at the implant site was considered as the complete restoration value (*i.e.*, 100% density restoration), while the first postoperative value acquired within 7-10 days after surgery was approximately defined as the baseline value (*i.e.*, 0% bone restoration). Thus, all absolute density measurements were rescaled and expressed as percentage, referred to as "relative density".

The uptake of contrast medium at the surgical site, referred to as “uptake”, was measured as the difference between the average density in the CE acquisition minus the average density in the non-CE acquisition.

Surgical endpoint

The scientific endpoint was set between 120 and 134 days from the surgical procedure. When the scientific endpoint was achieved, the animal was euthanized with an injection of 2.5 mL of potassium chloride (KCl) under general anesthesia obtained with inhalant isoflurane at 5% dosage. The mandible was then carefully removed, keeping the implant site protected and surrounded by a cuff of adjacent soft tissues.

Ex vivo imaging

The *ex vivo* radiological evaluation of the harvested specimens was performed by ultra-high-definition CT (SkyScan 1276 microCT system [Bruker, Belgium; voltage: 85 kV, current: 47 μA, isotropic voxel size: 10 μm]). On the images obtained, a region of interest (ROI) corresponding to the surgical defect repaired with the scaffold was manually identified through comparison with the first postoperative imaging. The software CT Analyser 1.17.7.2 (Bruker®) was used to extract quantitative data regarding the ROI (*i.e* bone volume as percentage of the overall tissue volume, trabecular density, trabecular thickness, and intertrabecular distance).

Specimen processing, staining, and histological imaging analysis

The surgical specimen, including the mandible and soft tissue surrounding the implanted sites, underwent a decalcification process with ethylenediaminetetraacetic acid (EDTA). Before paraffin embedding, each sample was cut at the level of scaffold’s midpoint, obtaining two specimens to be subsequently processed with paracoronal histological slices (*i.e.*, with the cutting plane perpendicular to the greatest axis of the mandibular body). The site of the scaffold was identified by 3D-printing an

actual-size mandibular model obtained from the first post-operative CT of each rabbit, thus comparing it to the harvested *ex vivo* mandibular specimen (3D Printer Dimension 1200es System Stratasys (Eden Prairie, MN, USA).

Histological sections were deparaffinized in xylene, rehydrated, and stained with H&E (Bio-Optica), to analyze general tissue morphology.

Statistical analysis

Statistical analysis was performed using RStudio (Version 1.2.5042). Two types of data were gathered for analysis: 1) time-dependent data and 2) endpoint data. The first cluster included relative density, and uptake, whereas the second entailed microarchitectural bone characteristics and histological bone characteristics. These data were considered as the response variables and association thereof with the following explanatory variables was checked: scaffold employment (yes *vs* no), scaffold seeding (yes *vs* no *vs* no reconstruction), stem cells seeding concentration (1000 cells/mm^3 *vs* 2000 cells/mm^3 *vs* 3000 cells/mm^3 *vs* controls), material (HyCh *vs* PLA-PCL-HyCh *vs* no reconstruction). Comparison between explanatory variable-determined subgroups was performed through analysis of variance with estimated marginal mean-based Tukey-adjusted *post hoc* test. Endpoint data were graphically rendered through violin plots and analyzed through the Mann-Whitney test (for dichotomous explanatory variables) and the Kruskal-Wallis test (for non-dichotomous explanatory variables). Significance was set at 0.05 for all statistical tests. P-values comprised between 0.05 (included) and 0.10 (excluded) were considered "close-to-significance".

Ethics

The protocols (AUP#6010; title: *Primary reconstruction of maxillary and mandibular defects with computer-aided designing, computer-aided manufacturing bioengineered composite scaffolds*) for experimentation on animals were approved by the University Health Network Animal Care

Committee (Princess Margaret Cancer Centre, University Health Network, University of Toronto) in April 2019.

Results

Rabbit mesenchymal stromal cells (rMSCs) (subchapter 2.1)

The relative density increase (RDI) curve presented a similar trend in rMSCs experimental group, compared to hMSCs group (baseline model; see Chapter 1), but reached an inferior value (*i.e.* less than 50% *vs.* 70% in 120 days) (Figure 3). Cell concentration at seeding showed an effect on RDI; 1000 cells/mm^3 concentration was associated with significantly higher RDI compared to 2000 and 3000 cells/ mm^3 (Figure 4). Nevertheless, final outcomes at 130 days were similar between the 3 different concentrations. Overall HyCh and PLA-PCL-HyCh did not show a significantly different RDI and enhancement uptake (HU) (Figure 5).

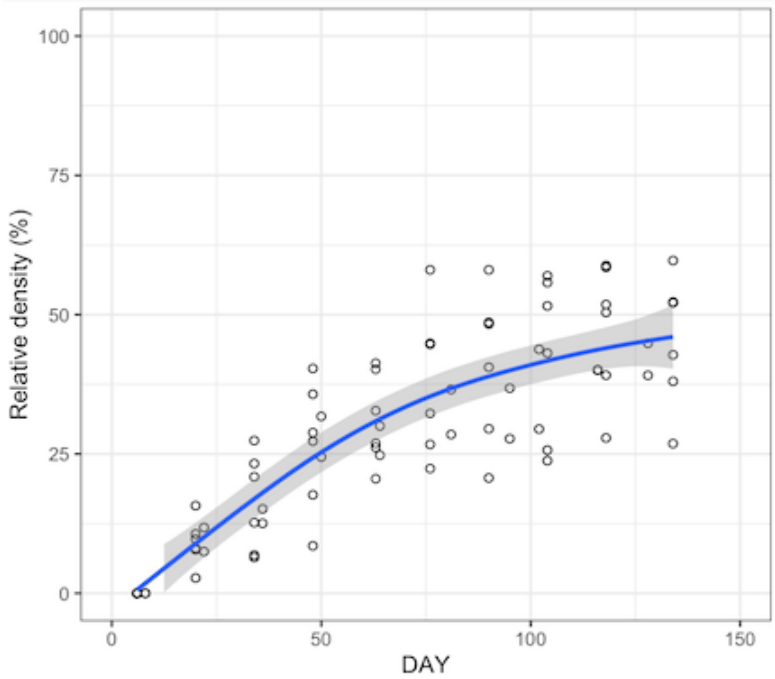

Figure 3 Relative density increase over time in rMSCs experimental group.

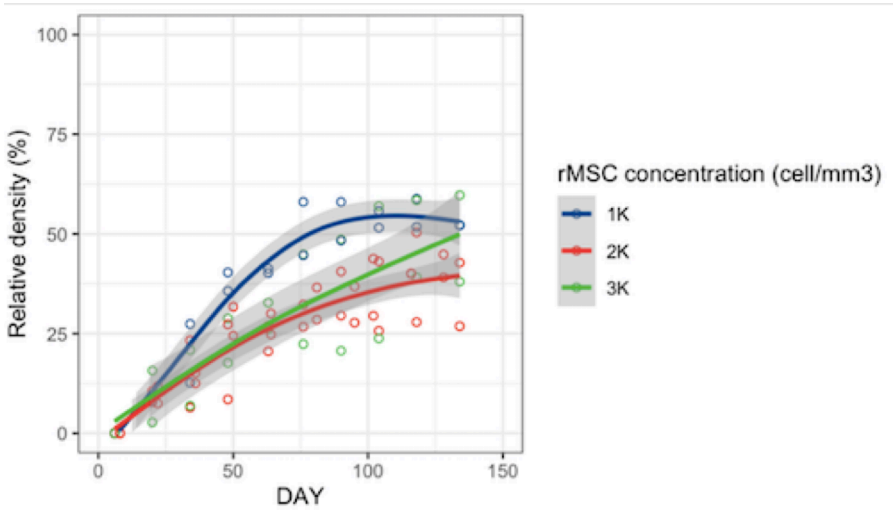

Figure 4 Relative density of the surgical site over time in rMSCs experimental group, stratified by cell concentration at seeding.

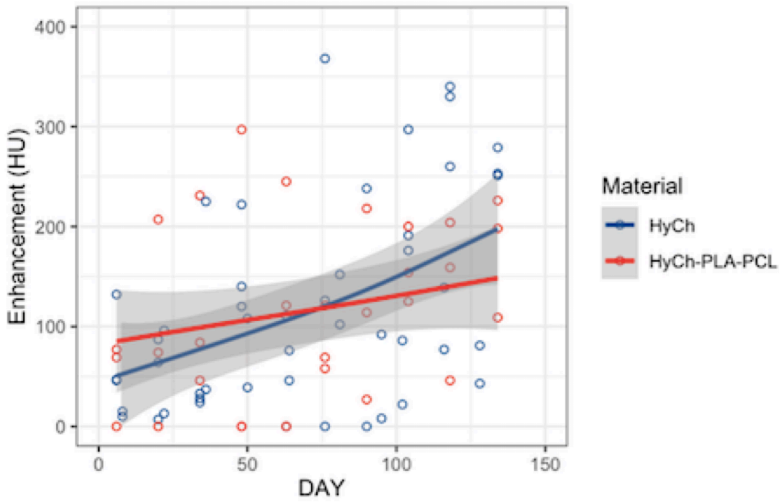

Figure 5 Relative density of the surgical site over time in rMSCs experimental group, stratified according to material composing the scaffold.

Bone morphogenetic protein 2 (BMP-2) (subchapter 2.2)

The relative density curve has showed a similar trend in hMSCs+BMP-2 experimental group, compared to hMSC group (baseline model; see Chapter 1) (Figure 6). Non seeded scaffolds resulted in a faster performance than the unseeded ones, this result in not statistically significant and the relative density value reached after 130 days is almost identical between seeded and unseeded groups (Figure 7).

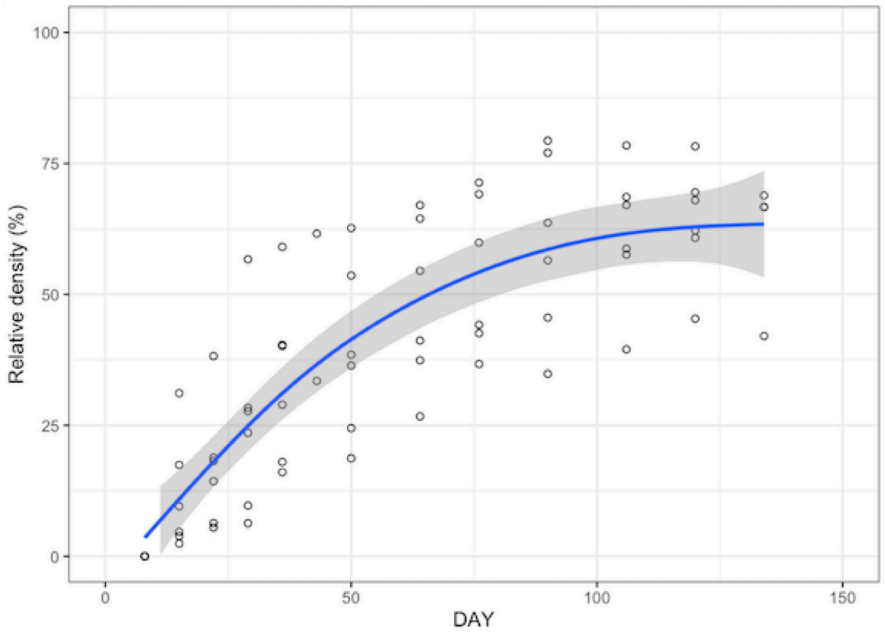

Figure 6 Relative density increase over time in hMSCs+BMP2 experimental group.

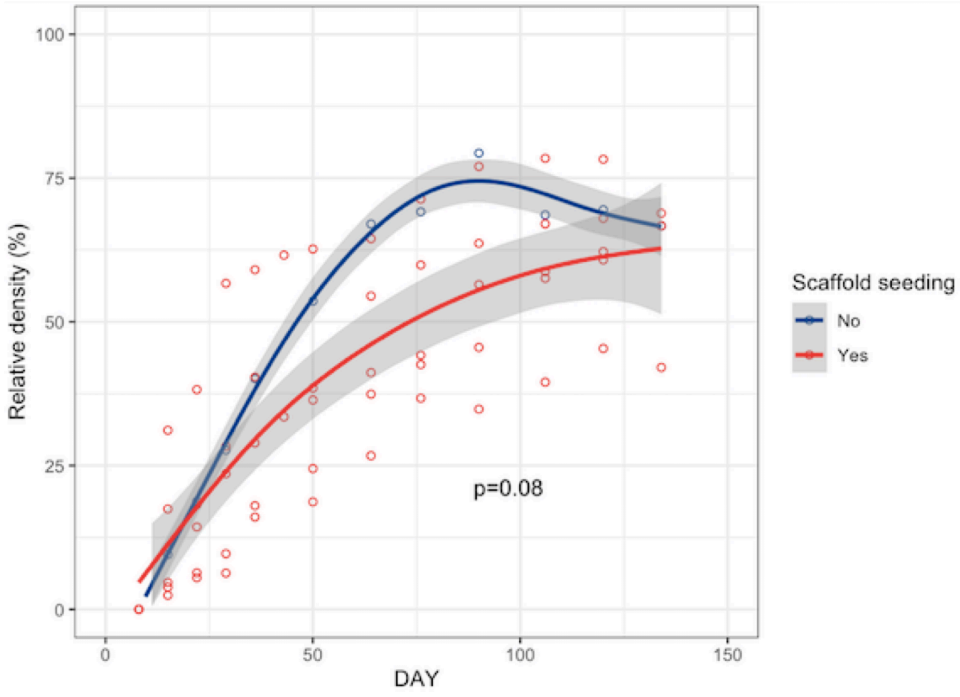

Figure 7 Relative density of the surgical site over time in hMSCs+BMP2 experimental group, stratified by employment of seeded *vs* unseeded scaffold.

Heterotopic bone formation (subchapter 2.3)

We did not observe any bone formation in scaffolds implanted in the subcutis, assed with radiological and histological tecniques.

Ex vivo results

HyCh seeded with rMSCs resulted in a slightly higher performance in terms of relative bone volume than PLA-PCL-HyCh, however not statistically significant (Figure 8). Bone characteristics did not show a significant difference between seeded scaffolds + BMP-2 as opposed to unseeded ones + BMP-2 (*i.e.* relative bone volume, trabecular density, trabecular thickness, and intertrabecular distance) (Figure 8). Heterotopic subcutaneous implant did not show bone growth (Figure 8).

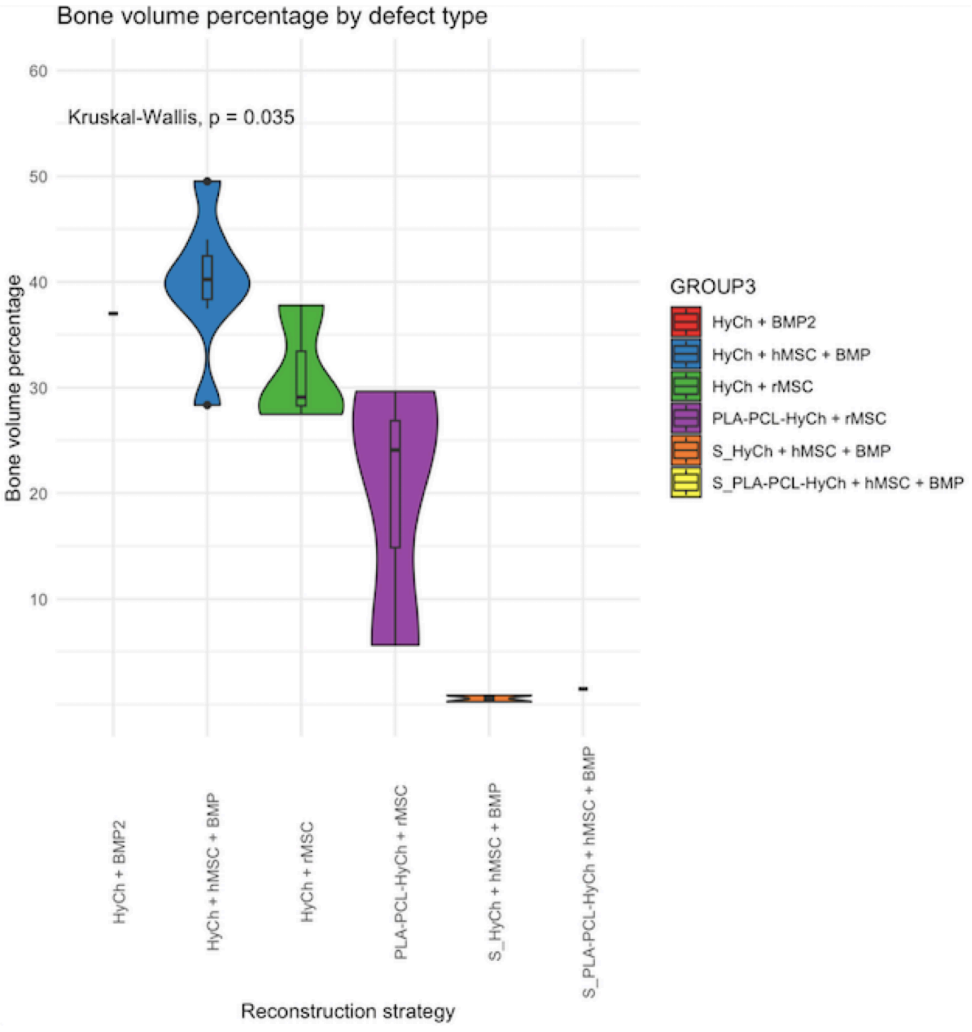

Figure 8 Violin plots showing that the microarchitectural characteristics of regenerated bone in terms of bone volume among study subgroups.

Discussion

In the rMSCs experimental group, the regenerative performance in terms of RDI did not overcome the result obtained in hMSCs group (baseline model; see Chapter 1), reaching a value of less than 50% in 120 days (*vs* 70% of the baseline model). Interestingly, cell concentration at seeding played a different role in rMSCs group: the lowest concentration (1000 cells/mm$^{3)}$ was associated with significantly better regeneration, compared to 2000 and 3000 cells/ mm^3. This result differs from what was seen in the baseline model, with opposite result. Overall HyCh and PLA-PCL-HyCh did not show a significantly different RDI and uptake enhancement (HU), again a different result than what observed in the baseline model. A possible explanation of these discouraging results could be the poor functioning of the seeded rMSCs. A recent publication by Ngeun *et al*[17]. demonstrated a notable drop in the proliferation rate and osteogenic differentiation capability of bone marrow rMSCs post-cryopreservation, and proved also that the viability, proliferation rate, and differentiation properties of adipose tissues MSCs remained higher than that of bone marrow MSCs after cryopreservation. Authors concluded that there are differences in morphology, differentiation potential, and resilience to cryopreservation among various animal models and humans and also among MSCs from different sources in the same species.

The regenerative performance, in terms of RDI, in hMSCs+BMP2 experimental group, was similar compared to the results in the hMSCs group (our baseline model). The dose administrated (5 μg) was the same proved to be optimal in regenerating an analogue mandibular defect of 5x5x2 mm in rats by DeConde *et al.*[18] Probably there is still room for improvement by modulating the local release kinetics of the stimulating factor: providing a low steady release of growth factors can entirely avoid the initial supraphysiologic burst, resulting in heterotopic bone formation and pleiotropic non-bone-specific effects. Of note, non-seeded scaffolds resulted in having a better performance than the unseeded ones; however it is worth mentioning that this is based on a single observation and therefore the interaction between MSCs and BMP-2 needs to be further investigated.

We did not observe any bone formation in scaffolds implanted in the subcutis. This result can suggest that bone regeneration is strictly linked to the surrounding microenvironment and the stimuli coming from the defect boundaries.

Strengths and limitations

The main strength of the present study is represented by the optimization methods used, being relatively simple, and enabling to exploit the expertise acquired with the baseline model.

The main limitation is represented by a reduced numerosity of samples in each experimental group.

Conclusions

Unfortunately, using rMSCs or BMP-2 we did not obtained a further improvement in the regenerative performance in respect to our baseline model. We believe that the optimal synergy between the different "ingredients" of the model still needs to be identify. One strategy that could be promising is to enhance the vascularization of the scaffold, and some proposals could be co-culture systems and the vascular and osteogenic growth factors.

References

1. Tollemar V, Collier ZJ, Mohammed MK, Lee MJ, Ameer GA, Reid RR. Stem cells, growth factors and scaffolds in craniofacial regenerative medicine. *Genes Dis*. 2016;3(1):56-71. doi:10.1016/j.gendis.2015.09.004

2. Yan X, Chen YR, Song YF, et al. Scaffold-Based Gene Therapeutics for Osteochondral Tissue Engineering. *Front Pharmacol*. 2020;10:1534. doi:10.3389/fphar.2019.01534

3. Neumann A, Kevenhoerster K. Biomaterials for craniofacial reconstruction. *GMS Curr Top Otorhinolaryngol - Head Neck Surg 8Doc08 ISSN 1865-1011*. Published online 2009. doi:10.3205/CTO000060

4. Levi B, James AW, Nelson ER, et al. Human Adipose Derived Stromal Cells Heal Critical Size Mouse Calvarial Defects. Capogrossi MC, ed. *PLoS ONE*. 2010;5(6):e11177. doi:10.1371/journal.pone.0011177

5. Chung MT, Liu C, Hyun JS, et al. CD90 (Thy-1)-Positive Selection Enhances Osteogenic Capacity of Human Adipose-Derived Stromal Cells. *Tissue Eng Part A*. 2013;19(7-8):989-997. doi:10.1089/ten.tea.2012.0370

6. Ueda M, Yamada Y, Ozawa R, Okazaki Y. Clinical case reports of injectable tissue-engineered bone for alveolar augmentation with simultaneous implant placement. *Int J Periodontics Restorative Dent*. 2005;25(2):129-137.

7. Yuan J, Cao Y, Liu W. Biomimetic Scaffolds: Implications for Craniofacial Regeneration. *J Craniofac Surg*. 2012;23(1):294-297. doi:10.1097/SCS.0b013e318241bae1

8. Hong P, Boyd D, Beyea SD, Bezuhly M. Enhancement of bone consolidation in mandibular distraction osteogenesis: A contemporary review of experimental studies involving adjuvant therapies. *J Plast Reconstr Aesthet Surg*. 2013;66(7):883-895. doi:10.1016/j.bjps.2013.03.030

9. Krebsbach PH, Gu K, Franceschi RT, Rutherford RB. Gene Therapy-Directed Osteogenesis: BMP-7-Transduced Human Fibroblasts Form Bone *in Vivo*. *Hum Gene Ther*. 2000;11(8):1201-1210. doi:10.1089/10430340050015248

10. Riew KD, Wright NM, Cheng SL, V. Avioli *, □ , J. Lou L. Induction of Bone Formation Using a Recombinant Adenoviral Vector Carrying the Human BMP-2 Gene in a Rabbit Spinal Fusion Model. *Calcif Tissue Int*. 1998;63(4):357-360. doi:10.1007/s002239900540

11. H. S, S. K, D. S, S. B. Demineralized bone matrix, bone morphogenetic proteins, and animal models of spine fusion: an overview. *Eur Spine J*. 2001;10(0):S122-S131. doi:10.1007/s005860100303

12. Varady P, Li JZ, Cunningham M, et al. Morphologic Analysis of BMP-9 Gene Therapy-Induced Osteogenesis. *Hum Gene Ther*. 2001;12(6):697-710. doi:10.1089/104303401300057423

13. Bostrom MPG, Camacho NP. Potential Role of Bone Morphogenetic Proteins in Fracture Healing: *Clin Orthop*. 1998;355S:S274-S282. doi:10.1097/00003086-199810001-00028

14. Cheng SL, Lou J, Wright NM, Lai CF, Avioli LV, Riew KD. In vitro and in vivo induction of bone formation using a recombinant adenoviral vector carrying the human BMP-2 gene. *Calcif Tissue Int*. 2001;68(2):87-94.

15. Gerhart TN, Kirker-Head CA, Kriz MJ, et al. Healing segmental femoral defects in sheep using recombinant human bone morphogenetic protein. *Clin Orthop*. 1993;(293):317-326.

16. Heckman JD, Boyan BD, Aufdemorte TB, Abbott JT. The use of bone morphogenetic protein in the treatment of non-union in a canine model. *J Bone Joint Surg Am*. 1991;73(5):750-764.

17. Koung Ngeun S, Shimizu M, Kaneda M. Characterization of Rabbit Mesenchymal Stem/Stromal Cells after Cryopreservation. *Biology*. 2023;12(10):1312. doi:10.3390/biology12101312

18. DeConde AS, Sidell D, Lee M, et al. Bone morphogenetic protein-2–impregnated biomimetic scaffolds successfully induce bone healing in a marginal mandibular defect. *The Laryngoscope*. 2013;123(5):1149-1155. doi:10.1002/lary.23782

CHAPTER 3: "Critical-size defects and segmental mandibulectomy"

Introduction

In our previous Chapters, we performed non-critical-size mandibular defects in rabbits, but translational research on biomaterials and regeneration of large bone defects in the mandible requires a preclinical model that accurately recapitulates the regenerative challenges present in humans. In the present Chapter we attempted to create a more challenging preclinical model with a larger mandibular defect. In literature, a marginal mandibulectomy of at least 10 mm in length and 6 mm in height is considered resulting in a critical-size defect for adult New Zealand rabbits[1].

The regeneration of segmental defects represent an interesting setting from a clinical translation standpoint. These defects are notoriously difficult to simulate in animal model, due to the elevate morbidity and the challenges in the post-operative setting, due to the limited tolerance of feeding tubes, and therefore a quick restoration of the oral feeding is mandatory. So far, literature has reported a single successful attempt to perform a segmental mandibulectomy in a rabbit model.[2]

Beside critical sized defects, we also explored the feasibility of the safe performance of a segmental mandibulectomy in the rabbit model.

Materials and Method

Study design (Subchapter 3.1): Critical-size marginal mandibular defect

A preclinical study on an immunocompetent animal model (New Zealand rabbit, *Oryctolagus cuniculus*; body weight: 3 kg or higher) was designed to analyze the bone regenerative properties of optimized bioengineered scaffolds (*i.e.*, PLA-HyCh hybrid-core-shell seeded with hMSCs at the concentration of 2000 cells/mm^3) in unilateral critical-size marginal mandibular defects (10x10x8 mm). Five rabbits were operated according to this protocol.

In addition to defect size, the other new variable tested in this chapter of the study was the innovative and improved scaffold composition. The engineering team of the University of Brescia was able to

produce a hybrid core-shell composite scaffolds with a 3D-printed PLA core and a gelatin-chitosan hydrogel shell (PLA-HyCH), with excellent mechanical properties. A medical grade PLA was gently provided by Poly-Med, Inc. for 3D-printing and core structures were designed as lattices with fixed struts and parallelepipedal holes, subsequently filled by the HyCH shell. Core design and build direction were chosen to resist bite forces at best. The result was a new scaffold made by medical-grade PLA lattices of elliptical cross-section with about 20 wt% hydrogel shell.

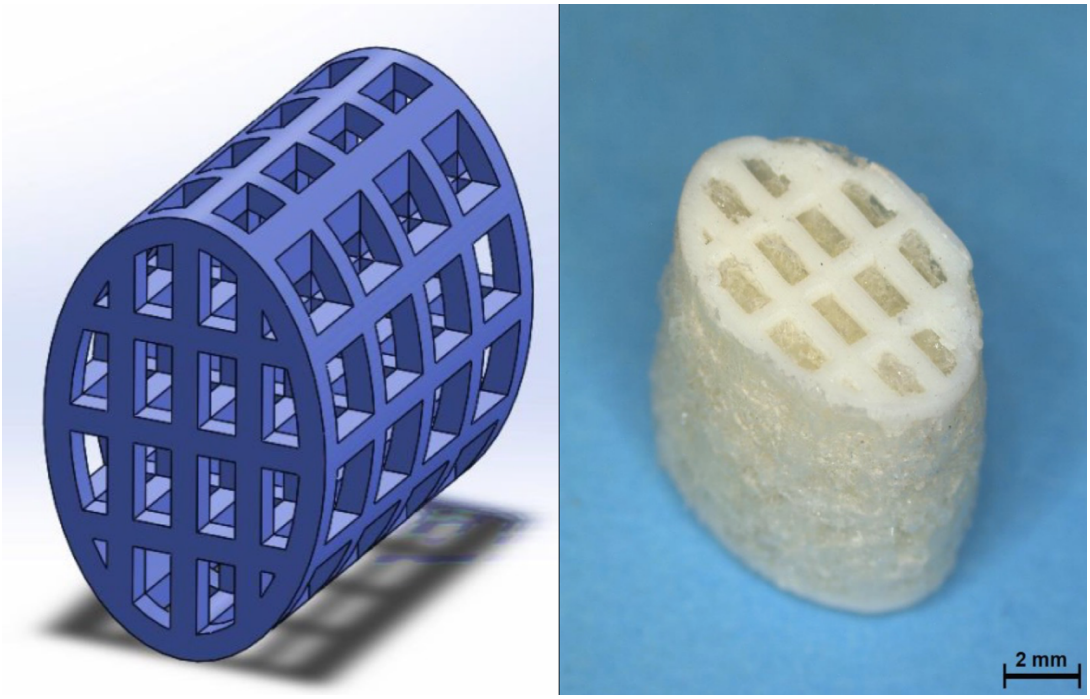

Figure 1 Hybrid core-shell composite scaffolds with a 3D-printed PLA core and a gelatin-chitosan hydrogel shell (PLA-HyCH).

Study design (Subchapter 3.2): Segmental mandibulectomy

A preclinical study on an immunocompetent animal model (New Zealand rabbit, *Oryctolagus cuniculus*; body weight: 3 kg or higher) was designed to analyze the feasibility of performing a segmental mandibulectomy, reconstructed with an unseeded PLA-HyCH hybrid-core-shell scaffold and fixation with resorbable PLLA-PGA-PDLA plate and screws. One rabbit underwent a unilateral segmental mandibulectomy.

For animal monitoring and adverse events assessment, *in vivo* imaging acquisition and analysis, specimen processing, statistical analysis, and ethics, the same protocols described in Chapter 1 and 2 were adopted.

The main steps of the procedure are summarized in Figure 1-4.

Results

Critical-size marginal mandibular defect (Subchapter 3.1)

The relative density increase (RDI) resulted 41% (range: 26-52%) in 120 days.

Segmental mandibulectomy (Subchapter 3.2)

A segmental unilateral mandibulectomy was successfully performed in the rabbit. The rabbit had no major adverse effect, no sign of infection, and the oral feeding was restored in the second day after surgery. The rabbit survived for 3 months without any major complication, except a late onset malocclusion.

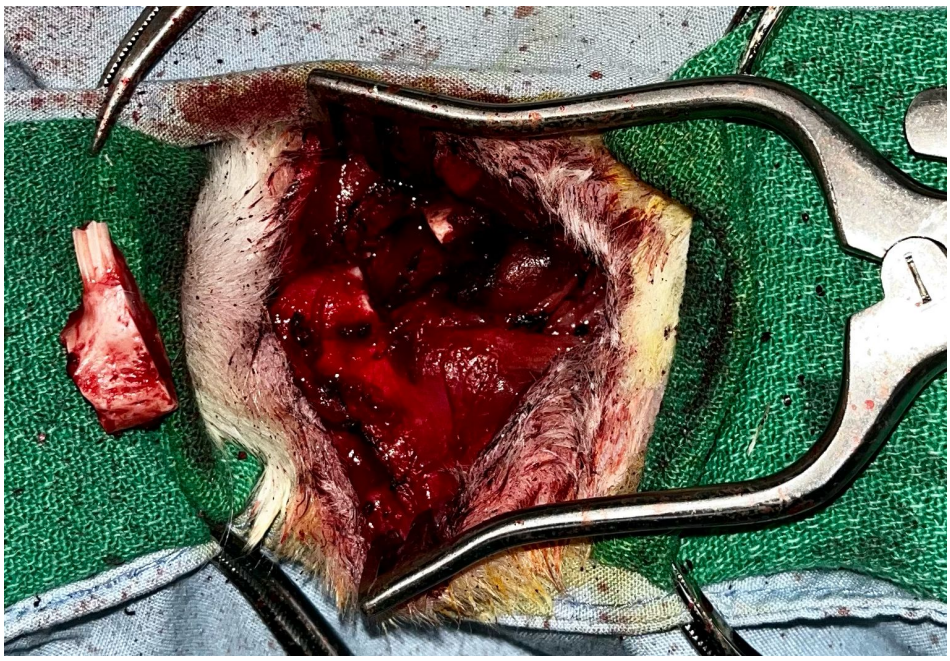

Figure 2 Left segmental mandibulectomy (segment length: 10 mm), the surgical defect and the specimen, including the first molar, are shown.

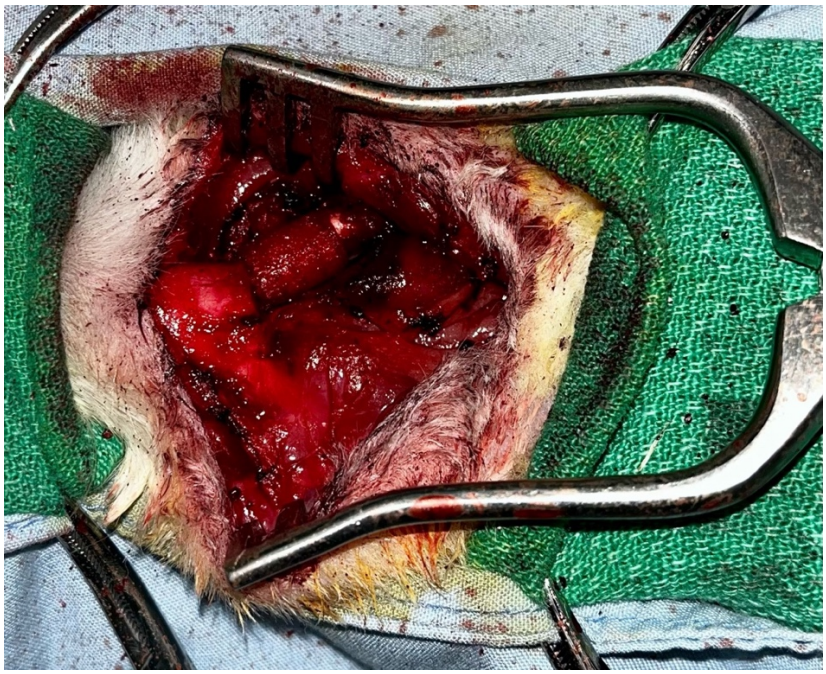

Figure 3 Left segmental mandibulectomy reconstructed by a hybrid core-shell composite scaffold.

Figure 4 Fixation of the mandibular stump and the scaffold with resorbable PLLA-PGA-PDLA plate and screws.

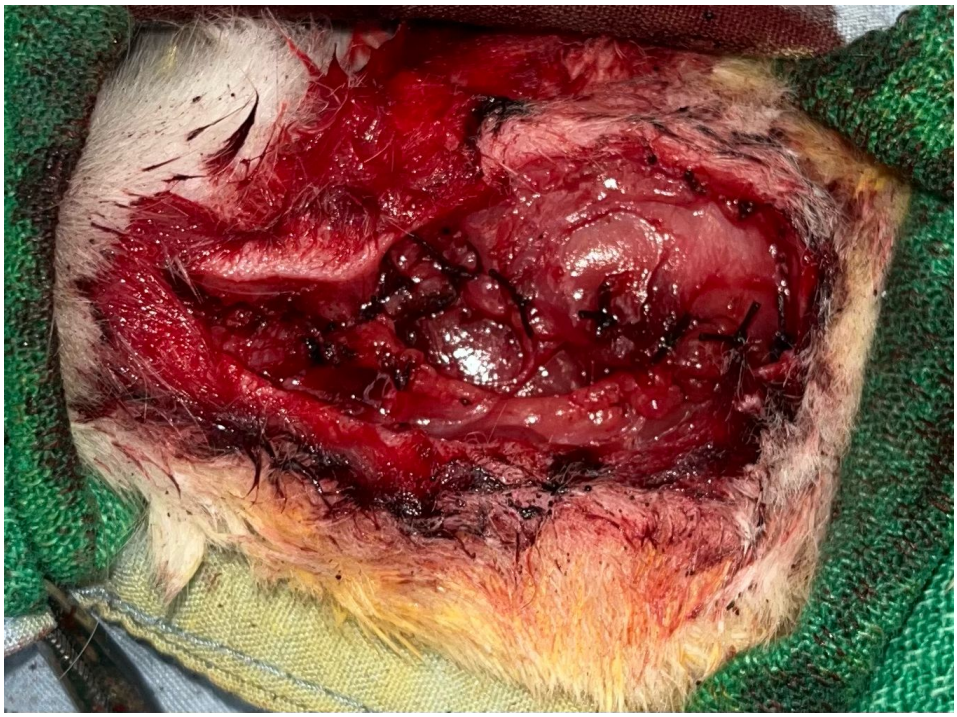

Figure 5 Suture of the suprahyoid muscles to cover the reconstructed area and the plate.

Discussion

The relative density resulted 41% (range: 26-52%) after 120 days, this result is corresponding to the regenerative performance of spontaneous regeneration in our baseline study in Chapter 1. The most likely explanation is that the regeneration process failed due to the displacement of the scaffold, this hypothesis was corroborated by the finding of the ex vivo analysis during the autopsy (Figure 5). In literature it is well-known that the matching between the surfaces of the scaffold and boundaries of the defect is recognized as key factor to allow new bone formation[3]

Figure 6 *Ex vivo* analysis proving the displacement of the scaffold, due to insufficient fixation at level of the surgical defect.

We succeed in performing a segmental mandibulectomy in the rabbit, with no major adverse effect: no sign of infection was detected, and the oral feeding was restored in the second day after surgery. The rabbit survived for 3 months without any major complication, except a late onset malocclusion. Lopez *et al.* described the feasibility of performing a segmental mandibulectomy and reconstruction with a 3D-printed bioactive ceramic in the rabbit, but authors only performed a centimetric defect

located in the anterior portion of the mandible without removing any molar rabbit and 33% of operated rabbits had a severe infection of the surgical site and were euthanized.[2] Our finding is based only on one experiment and it need to be replicated.

The term “critical size” refers to any size defect that does not heal over a specified time period. We reproduced a marginal mandibulectomies of 10 mm in length and 8 mm in height and marginal mandibulectomy of 10 mm in length. Those defects resulted to be “critical size” for adult New Zealand rabbits, according to the criteria of the literature,[1] but still remain limited if compared with the clinical analogous of at least 4 cm long mandibular segmental defect that might typically be seen in the human scenario.

Conclusions

We obtained a proof of concept of the pivotal role of matching between the surfaces of the scaffold and boundaries of the defect.

Our preliminary experience of the segmental mandibulectomy reconstructed with the new hybrid-core-shell composite scaffold showed a safe outcome profile and it needs to be investigated with further experiments.

References

1. Shah SR, Young S, Goldman JL, Jansen JA, Wong ME, Mikos AG. A composite critical-size rabbit mandibular defect for evaluation of craniofacial tissue regeneration. *Nat Protoc*. 2016;11(10):1989-2009. doi:10.1038/nprot.2016.122

2. Lopez CD, Diaz-Siso JR, Witek L, et al. Three dimensionally printed bioactive ceramic scaffold osseoconduction across critical-sized mandibular defects. *J Surg Res*. 2018;223:115-122. doi:10.1016/j.jss.2017.10.027

3. Bowers CA, McMullin JH, Brimley C, Etherington L, Siddiqi FA, Riva-Cambrin J. Minimizing bone gaps when using custom pediatric cranial implants is associated with implant success. *J Neurosurg Pediatr*. 2015;16(4):439-444. doi:10.3171/2015.2.PEDS14536

CHAPTER 4: "Development of a model of irradiated bone and osteoradionecrosis. Analysis of bone regeneration in the irradiated setting"

Introduction

Radiotherapy (RT) plays a crucial role in head and neck oncology, representing both a definitive treatment option, alone or in combination chemotherapy, and an adjuvant treatment option after surgery.[1,2] However, it comes with some drawbacks, due to the possible sequelae that can occurs after the treatment. Osteroadionecrosis (ORN) represents one of the most serious and complex sequelae of RT; in particular, mandibular ORN (mORN) can dramatically impact on the quality of life of patients treated for head and neck tumor.

With the present study, the research team aimed to: (i) develop a preclinical model of irradiated bone and osteradionecrosis and (ii) test the use of bioengineered scaffolds seeded with hMSCs in this setting, being aware of the extreme complexity represented by these models.

Materials and Method

Nine rabbits (white New Zealand rabbit) were irradiated at the level of the lower portion of the left mandible, using an X-Ray 225 Vp machine. The dose used was 7 Gy for each fraction, 5 fractions, one every two days, (35 Gy total dose for each rabbit). Since a 2D irradiation was performed, it has been estimated that even the right mandible was included in the irradiation field, receiving a dose of about 5 Gy . A 10x10mm square base collimator was used to limit toxicities to surrounding tissues, targeting the area with epicenter at the level below the root of the left mandibular first molar. Before each irradiation fraction, a cone-beam CT scan was performed to identify the established target area. The irradiation protocol was affixed to 9 the rabbits. The animals were then monitored both clinically with oral cavity inspection under general anesthesia every two weeks and radiologically every month (at weeks IV, VIII, XII and XVI after irradiation), altering CT and MRI methods always with and without contrast medium. These CT and MRI imaging were studied and analyzed with an expert

radiologist dedicated to head and neck pathology (Prof. Roberto Maroldi), to assess presence of signs of osteoradionecrosis was also confirmed.

Surgery performed approximately 4 months after irradiation. A mandibular defect of 5x5x5mm diameter was performed bilaterally in each rabbit. At the time of the surgery the irradiated rabbits were randomly divided into 3 groups: 1) in 2 rabbits, defects were not reconstructed; 2) in 3 rabbits, defects were reconstructed with PLA-HyCh hybrid core-shell scaffold alone; 3) in 3 rabbits, defects were reconstructed with PLA-HyCh hybrid core-shell scaffold seeded with hMSCs (concentration 3000 cells/mm3).

The resected bone was removed and analyzed with histological examination by an expert anatomopathologist dedicated to head and neck pathology (Dr. Lara Alessandrini), to assess the presence of signs of osteoradionecrosis.

Subsequently, the rabbits were followed with the same protocol adopted for the baseline model, with serial evaluation every 2 weeks with CT with and without iodinated contrast medium.

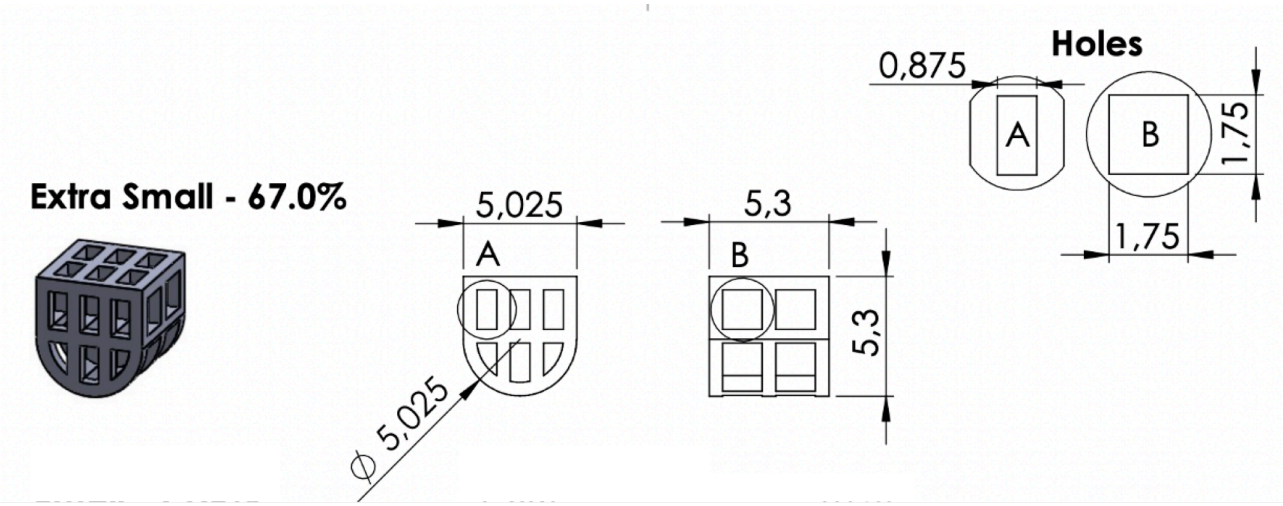

Figure 4.1 Details of the design of the small-sized hybrid core-shell scaffold (diameters 5x5x5mm) implanted in the context of rabbit jaw area undergoing radiotherapy.

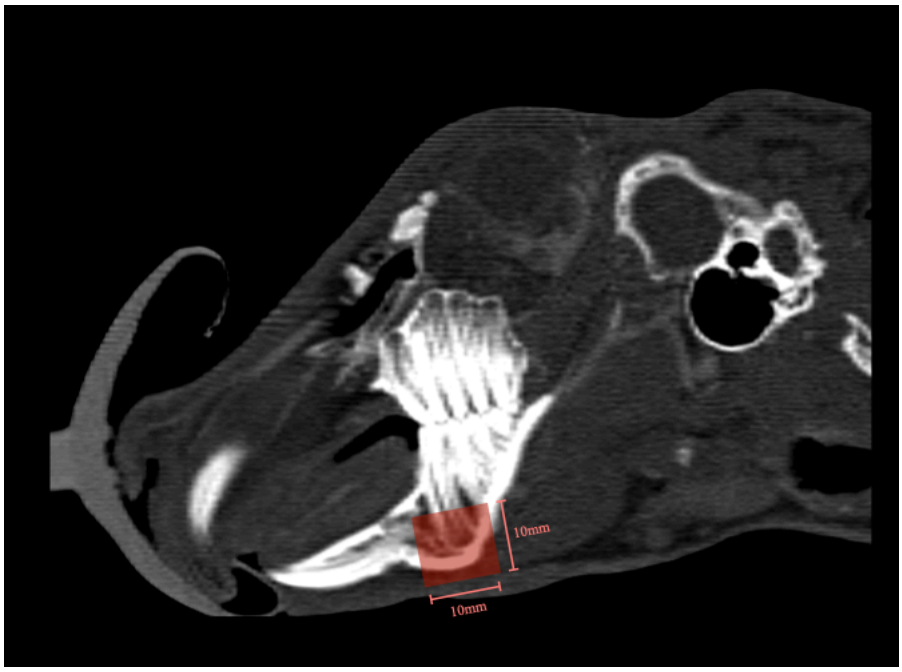

Figure 4.2 Two-dimensional target of radiotherapy treatment at level of the left side mandible on CT imaging (irradiated area is demarcated by the red square).

Results

In the post-irradiation period, no major events related to radiation treatment were recorded in the whole series. After the 3rd radiation fraction, 3 rabbits (33%) showed the first signs of mild alopecia in the submandibular region, without complete hair loss. All rabbits showed alopecia of different degree 4 months after radiation, but no skin lesions or signs of suprainfection occurred. Furthermore, there was no case of mucosal lesions and ulcers of the oral cavity or bone exposure at the irradiated mandibular regions. The entire population maintained adequate oral nutrition, without weight loss.

Unfortunately, at week VIII a death was recorded during the MRI examination of a rabbit, which did not wake up after the procedure (an event described and already recorded several times in other experimental group after general anesthesia in rabbits).

Overall, the first signs suggestive of ORN were evident at week IV, evident in 25% of cases; at week XVI all animals (100%) had signs suggestive of ORN. Specifically, radiological signs of severe ORN were described at week XII in 50% of cases, and in 75% at week XVI. Notably, ORN

signs were evident just on the left side of the mandible, which is the side irradiated with the higher dose (7 Gy/fraction). Whereas, histological signs of post-actinic damage were present and pronouncedly represented in all specimens examined, in both sides of mandible.

In the postoperative phase, all animals showed an increase in density relative (RDI) to the surgical site over the observation time. Considering the whole sample, postoperative RDI averaged 25.8% 165 days after surgery. Relative density analysis, according to irradiation dose, showed no statistically significant differences between the side irradiated with high dose and low dose (p-value = 0.9). Both groups achieved approximately 25% bone regeneration at 165 days after surgery. Specifically, the side irradiated with 5 Gy dose/fraction achieved 26.4%, the side irradiated with 7 Gy dose/fraction achieved 25.2% bone regeneration.

Considering the type of reconstruction, instead, RDI was significantly more pronounced in the group in which the defect was not reconstructed with scaffold or with scaffold seeded with stem cells (p-value < 0.001), reaching an overall 57.3% bone regeneration at 165 days after surgery (Figure 4.3). Further analyzing the population in which scaffold was used for defect reconstruction, it was observed that the use of stem cells was associated with a statistically significant increase in RD compared with scaffold-only reconstruction, reaching approximately 29.9% bone regeneration at 165 days after reconstruction (*vs.* 11.2% with scaffold alone, p-value < 0.001) (Figure 4.3).

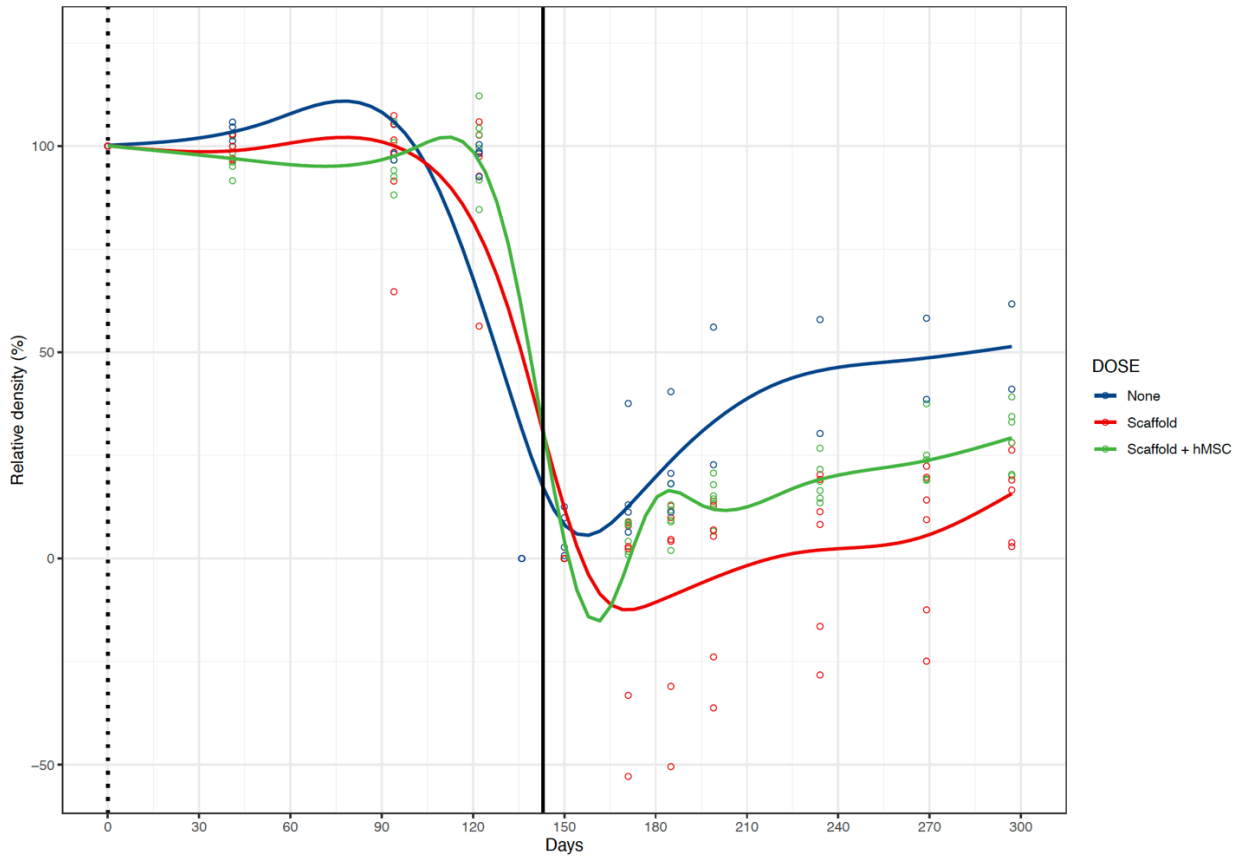

Figure 4.3 Graphical representation of the trend in relative density of the surgical site over time from before the start of radiotherapy to the time of euthanasia (the time of surgery is represented by the black vertical line), stratified by the type of reconstruction (no reconstruction *vs*. unseeded *vs*. seeded scaffold).

Discussion

The literature offers several models of mandibular osteoradionecrosis, which widely differ in terms of animal model, irradiation regimen, and irradiation dose. In particular, in terms of rabbits animal model studies are rather limited and there is some variability in terms of both dose and irradiation regimen used. For these reasons, it is not yet possible to speak of a well-defined preclinical model of mandibular ORN.[3,4]

On CT examination, features such as empty lacunae, presence of cortical erosion, unilateral or bilateral in more advanced cases, the loss of bony trabeculae, and the presence of osteolytic lesions or bone sequestrum are considered indicative for ORN. In the side irradiated with the higher dose, the entire sample had characteristic signs of radiological ORN at week XVI, and signs of severe bone

damage were observed in 75% of cases. In contrast, the mandibular side irradiated with lower dose (5Gy/fraction) showed no radiological evidence suggestive of ORN, throughout the entire of follow-up. Therefore, these data suggest that 7 Gy/fraction, for 5 fractions, is the dose capable of inducing ORN radiologically evident, whereas the dose of 5 Gy/fraction did not appear to be sufficient to induce damage radiologically visible.

The relative density (RD) of the irradiated target area during the post-irradiation phase was also calculated. The results obtained, however, didn't show significant changes in bone density between the low-dose or high-dose irradiated group in this phase. This method, in this specific setting, resulted to be unsuitable in detecting the underlying bone changes. The first hypothesis is that, in addition to osteorarefaction phenomena such as cortical erosion and loss of trabeculae, irradiation also induce bone alterations that include osteo-inductive phenomena such as bone sclerosis. Therefore, it is possible that the concomitance of the two phenomena resulted in a flat trend of RD. A second hypothesis is that the RD estimation method used is not sensitive enough to identify bony changes, which are appreciable on qualitative evaluation of radiological images instead.

Histologically, both fractional doses of irradiation, 5 Gy and 7 Gy, showed significant bone damage, with significant signs of bone necrosis in both sides with the same grade of severity.

In view of the radiological and histological evidence, we believe that the protocol tested and developed by our research group allowed the development of a dual model. On one hand, in the hemi-mandible ipsilateral to the irradiation source, receiving 7 Gy/fraction, a model of osteoradionecrosis was obtained, where there was evidence of radiological damage, in the absence of mucosal ulceration or other possible severe clinical changes. On the other hand, in the hemi-mandible contralateral to the irradiation source, but included within the irradiation cone and receiving 5 Gy/fraction, a model of irradiated bone was obtained, defined as such by the absence of radiologic and clinical evidence of damage, but characterized by the presence of histologic signs of bone remodelling and necrosis.

Up to date, several animal models have been developed to study ORN, such as murine, rodent, canine, and porcine models. Among the various models proposed in the literature, the rabbit animal

model is advantageous both compared with models such as the murine or rodent model because of its size and "strength," allowing an adequate clinical evaluation and a sufficiently extended follow-up over the time; and also compared with larger models (*e.g*. canine model) because of an easier handling, manageability, lower cost, and thus enabling the possibility of studying a larger sample size. An additional advantage of using the rabbit model lies in the fact that this model is characterized by a bone turnover 3 times faster than human bone turnover, allowing the possibility of reducing the follow-up time, therefore, what is observed in a 6-month time frame in the rabbit can be considered corresponding to what happens in the human setting in about 2 years.[5]

The developed model showed a very good safety profile, achieving the desired radiotherapy-induced toxicity, the osteoradionecrosis, and at the same without compromising the model itself with excessive toxicity (radiation-specific mortality was 0%). Thus, the model developed was safe and easily feasible, and it can be considered a valid and reproducible experimental model. Finally, this model can be considered a a valid model for studying radiation therapy-induced effects, for two different doses, allowing maximum optimization of resources and costs.

Up to date, very few authors have investigated bone regeneration in a radionecrotic bone setting. This setting is extremely unfavorable for tissue regeneration given the known histomorphological damage and functional impairment of the bone microenvironment, characterized by impaired microcirculation, resulting in hypoxia and hypocellularity, and tissue fibrosis. It is therefore more difficult to compare the few data existing, given the diversity of the models tested both in terms of animal models, extent of damage obtained, and type of scaffolds and stem cells used.

In the present study, bone regeneration performance in the context of irradiated bone was about 25 percent over 165 days. The percentage of tissue regeneration was significantly reduced compared to what was observed in non-irradiated bone settings, both in terms of spontaneous bone regeneration and in terms of bone regeneration adjuvanted using bioengineered scaffolds, whether seeded or not with stem cells.

The increase in relative density showed no statistically significant differences between high-dose and low-dose irradiated models; therefore, the bone regeneration performance after irradiation with 5 Gy/fraction did not exceed the extent of regeneration observed in bone irradiated with 7 Gy/fraction dose. Although radiologically clear differences were observed in terms of bone alteration between the two sides, that were completely absent in the right side (lower dose irradiation) and, on the contrary, markedly evident in the left side (higher dose irradiation), histologically, this difference was not confirmed as well, as in all analyzed specimens were described signs of marked bone damage. Therefore, the result obtained in terms bone regeneration, that resulted to be comparable between the two groups, is consistent to what has been observed histologically, where the bone microenvironment is, in both sides and equally, diffusely characterized by elements that make the environment particularly unfavorable for tissue regeneration, such as hypocellularity, hypovascularization and fibrosis.

In cases where the defect was not reconstructed, the increase in relative density was significantly greater than that observed in defects reconstructed with scaffolds or scaffolds seeded with stem cells, reaching 57.3% regeneration of the bone defect at 6 months. Therefore, the data showed that bone regeneration was not favored by the presence of a scaffold in the context of irradiated bone, unlike what has been reported in other studies proposed in the literature.[6] When defects were reconstructed with scaffolds, a significant increase in relative density was observed when the scaffolds were seeded with hMSCs (3000cell/mm3). However, the bone regeneration achieved by using scaffolds seeded with hMSCs did not exceed 30% at 6 months after surgery. Currently, in the context of radionecrotic bone, there are still few studies regarding the use of scaffolds and stem cells; however, among these are several studies that demonstrate both the safety in the use of stem cells in the context of irradiated bone and their promising role in bone regeneration, hypothesizing a possible role of stem cells in this context of tissue hypocellularity.[6] Among them, the study by Thery *et al*. demonstrated how in irradiated rat model the use of tricalcium phosphate scaffolds and bone marrow stem cells stimulates bone regeneration.[7] However, the irradiation setting

tested was calculated to be the equivalent of 60 Gy, a much lower dose than the setting tested by our research group (estimated biological dose equivalent: 115 Gy). However, although some authors have obtained promising results, the data in this specific setting still remain very discordant.[8]

Although in terms of bone regeneration the result obtained in this study was not satisfactory, there are some important aspects to consider. *In primis*, the use of scaffolds and scaffolds seeded with stem cells demonstrated an adequate safety profile. In all rabbits in which the defect was reconstructed, no adverse events related to their use were observed throughout the follow-up, either in terms of local suprainfection or in terms of progression of the osteoradionecrosis process in the areas surrounding the scaffold. Whereas, only one complication has been documented in the postoperative phase (70 days after surgery): one rabbit developed a swelling of the left mandible with suprainfection that didn't heal with medicaments and therefore; notably, this rabbit belonged to the group that was not reconstructed with scaffold. *In secundis*, the postoperative follow-up was performed for 6 months, a rather extended time frame that hasn't been reached by any other study in the literature so far for an ORN model. This observation period can be considered, in relation to the rabbit model, a sufficiently long time to establish and define this model as "safe."

Currently, the use of scaffolds in the regenerative setting has yielded limited results, and there is therefore ample room, as well as a need, for further studies to optimize the role of both scaffolds and stem cells in this setting. In addition, the use of biomaterials in the treatment of ORN could also be applied for other declinations, such as the use as delivery devices for the local and gradual, controlled, and prolonged release of anti-ORN drugs. To note, in this area, some research groups have achieved interesting and promising results using bioengineered scaffolds as carriers for therapy.[9]

Study limitations

To conclude, one limitation of the study is the small sample size. Since this was a pilot study for ORN model development, and given the limited evidence in the literature, the choice was consequent to the need to first verify the safety of the irradiation doses used. The results obtained require to be validated by subsequent studies, including by increasing the sample size.

Conclusions

With this chapter we obtained a valid animal model of mandibular osteoradionecrosis with an excellent correlation between dose and biological damage. From the regenerative standpoint, the scaffold-MSC tested did not seem to highly catalyze the bone repair of bone defects in the osteoradionecrotic region.

References

1. Chronopoulos A, Zarra T, Ehrenfeld M, Otto S. Osteoradionecrosis of the jaws: definition, epidemiology, staging and clinical and radiological findings. A concise review. *Int Dent J*. 2018;68(1):22-30. doi:10.1111/idj.12318

2. Marx RE. Osteoradionecrosis: A new concept of its pathophysiology. *J Oral Maxillofac Surg*. 1983;41(5):283-288. doi:10.1016/0278-2391(83)90294-X

3. Xu J, Zheng Z, Fang D, et al. Mesenchymal Stromal Cell-Based Treatment of Jaw Osteoradionecrosis in Swine. *Cell Transplant*. 2012;21(8):1679-1686. doi:10.3727/096368911X637434

4. Eppley BL, Connolly DT, Winkelmann T, Sadove AM, Heuvelman D, Feder J. Free Bone Graft Reconstruction of Irradiated Facial Tissue: Experimental Effects of Basic Fibroblast Growth Factor Stimulation. *Plast Reconstr Surg*. 1991;88(1):1-11. doi:10.1097/00006534-199107000-00001

5. Abu-Serriah MM, McGowan DA, Moos KF, Bagg J. Extra-oral craniofacial endosseous implants and radiotherapy. *Int J Oral Maxillofac Surg*. 2003;32(6):585-592. doi:10.1054/ijom.2003.0429

6. Gundestrup AK, Lynggaard CD, Forner L, et al. Mesenchymal Stem Cell Therapy for Osteoradionecrosis of the Mandible: a Systematic Review of Preclinical and Human Studies. *Stem Cell Rev Rep*. 2020;16(6):1208-1221. doi:10.1007/s12015-020-10034-5

7. Jin IG, Kim JH, Wu HG, Kim SK, Park Y, Hwang SJ. Effect of bone marrow-derived stem cells and bone morphogenetic protein-2 on treatment of osteoradionecrosis in a rat model. *J Cranio-Maxillofac Surg*. 2015;43(8):1478-1486. doi:10.1016/j.jcms.2015.06.035

8. Thery A, Bléry P, Malard O, et al. Role of the stromal vascular fraction from adipose tissue in association with a phosphocalcic scaffold in bone regeneration in an irradiated area. *J Cranio-Maxillofac Surg*. 2015;43(7):1169-1176. doi:10.1016/j.jcms.2015.05.014

9. Daniel M, Luby AO, Buchman L, Buchman SR. Overcoming Nuclear Winter: The Cutting-edge Science of Bone Healing and Regeneration in Irradiated Fields. *Plast Reconstr Surg - Glob Open*. 2021;9(6):e3605. doi:10.1097/GOX.0000000000003605

CHAPTER 5: "Interaction between a regenerative model and malignant tumor cells"

Introduction

Data regarding interaction of human mesenchymal stroma cells (hMSCs) and tumor cells are scarce. However, it is reported that tumor has the ability to guide MSCs to migrate into the tumor tissue, becoming enriched in MSCs. There are no relevant evidence available regarding the mechanism of distribution and differentiation of MSCs in tumor tissue and on the effect on tumor growth after MSCs engrafting in tumor tissue. Zhao *et al.*[1] observed that MSCs can accelerate the tumor development and can differentiate into myofibroblast under the induction of tumor microenvironment. In addition, experiments indicate that MSCs can modulate the immune system through various routes (inhibition of the differentiation of monocytes to dendritic cells, and the proliferation of B cells; alteration of the phenotype of NK cells and suppress proliferation, cytokine secretion, and cyto-toxicity).[2–4]

We believe that it is pivotal to assess if the use of MSCs, at concentrations needed for regenerative purposes, can be considered safe when we applied after a malignant tumor ablation.

Materials and Method

Study design

A preclinical study on an immunocompetent animal model (New Zealand rabbit, *Oryctolagus cuniculus*; body weight: 3 kg or higher) was designed to analyze the interaction between VX2 tumor and a bioengineered scaffold seeded with hMSCs. We evaluated the loco-regional control after tumor resection. Rabbit VX2 head and neck squamous cell model is derived from the cottontail rabbit papilloma virus, which, like the human papilloma virus (HPV), participates in papillomatosis and carcinogenesis of squamous epithelium, and resulted a good model for translational head and neck research[5]. The hybrid core-shell composite scaffolds were seeded with different concentrations of hMSCs, namely 1000 and 3000 cells/mm3. VX2 tumor cell suspension was prepared by passing 1 cm^3 of VX2 tumour through a 100 μm filter using PBS and 0.3 mL of VX2 tumor suspension were

injected proximal to the inferior border of the mandible. Tumor growth was monitored through serial clinical and radiological examinations over 10 days, when the size of the tumor nodule reached about 0.5 cm of diameter. Then surgical gross-total resection of the paramandibular lesion was performed, followed by marginal mandibulectomy to remove the bone adjacent to the tumor. The surgical bone defect was reconstructed with the bioengineered scaffold.

The rabbits were followed up with weekly clinical and radiological evaluation.

Figure 1 Specimen of the resected paramandibular tumor.

Results

Three rabbits underwent a gross total resection of the tumor, according to this protocol.

After the operation, there was no evidence of loco-regional recurrence within a month. All of them developed pulmonary distant metastasis.

Discussion

In the present pilot study, any local or regional recurrence was registered, but a sudden development of distant metastasis (lung) was observed in 100% of the series. This raised some doubts about safeness of injections used. Our group already has an extensive experience with rabbit VX2 models,[5]

and usually the biological behavior of this animal model closely resembles that of human head and neck squamous cell carcinoma. Moreover, it also closely resembles HPV mediated head and neck squamous cell carcinoma. The consistent growth of the tumor along with the high rates of cervical metastasis make it a useful model for assessing treatment regimens targeting both the primary and nodal metastasis.

We still need to clarify whether a local immune response may impact on immune surveillance and contribute to distant failure or a different issue (*e.g.* injection into small blood vessels) occurred . Therefore, the group intends to repeat the experiment, increasing the number of the sample size and including a control group with unseeded scaffold, in order to (i) compare the disease specific survival, loco-regional control, and distant metastases free survival between the 2 groups, and (ii) to clarify the role of MSCs in supporting tumor relapse.

Conclusion

This Chapter addresses a fundamental issue such as the introduction of hMSC into an environment where malignant cells are potentially present. The need to demonstrate the safety in terms of local tumor recurrence has been long debated. Yet again, this represents a pilot study with limited population. However, we obtained interesting results, as local or regional recurrence did not occur.

Unfortunately, limited remarks can be pointed out with the present sample size as data obtained are insufficient to lead to any strong conclusion. Our preliminary results need to be validated by subsequent studies, both increasing sample size and including a control group to perform oncological outcome comparison.

References

1. Zhao HF, Chen J, Xu ZS, Zhang KQ. Distribution and differentiation of mesenchymal stem cells in tumor tissue. *Chin Med J (Engl)*. 2009;122(6):712-715.

2. Jiang XX, Zhang Y, Liu B, et al. Human mesenchymal stem cells inhibit differentiation and function of monocyte-derived dendritic cells. *Blood*. 2005;105(10):4120-4126. doi:10.1182/blood-2004-02-0586

3. Corcione A, Benvenuto F, Ferretti E, et al. Human mesenchymal stem cells modulate B-cell functions. *Blood*. 2006;107(1):367-372. doi:10.1182/blood-2005-07-2657

4. Sotiropoulou PA, Perez SA, Gritzapis AD, Baxevanis CN, Papamichail M. Interactions Between Human Mesenchymal Stem Cells and Natural Killer Cells. *Stem Cells*. 2006;24(1):74-85. doi:10.1634/stemcells.2004-0359

5. Muhanna N, Douglas CM, Chan HHL, et al. Rabbit VX2 head and neck squamous cell models for translational head and neck theranostic technology development. *Clin Transl Med*. 2021;11(10):e550. doi:10.1002/ctm2.550

CONCLUSIONS AND FUTURE DIRECTION OF THE RESEARCH

In these three years, we achieved several successes: we demonstrate that bone regeneration can be boosted by scaffold- and seeded scaffold-reconstruction, achieving, respectively, 50% and 70% restoration of presurgical bone density in 120 days, compared to 40% restoration seen in spontaneous regeneration. At the same time we also faced with some important failures. Nevertheless, this did not, and does not discourage us, as it is part of research process, especially when pursuing ambitious goals.

The development of scaffold-mediated bone regeneration is a great challenge, in particular in the head and neck region. Evidence of the effectiveness of our baseline regenerative model are promising, although the model still needs to be improved in terms of speed and amount of bone restored. We are proud of the remarkable progress in materials engineering that in just a few years has brought improve scaffold composition and structure.

Our next step will be guided by the results obtained by two systematic reviews ongoing, inherent to the following critical areas: 1) cell co-cultures for bone regeneration, as there is some evidence that suggest that the combining the seeding of mesenchymal stem cells with endothelial stem cells can promote vascularization of the newly formed bone; 2) growth factors, there is some evidence that certain growth factors can significantly boost bone regeneration, and therefore we need to identify which is the best and ideal dose to use to achieve the desired biological effect.